Check for updates

AGU ADVANCING EARTH AND SPACE SCIENCE

Water Resources Research

RESEARCH ARTICLE
10.1029/2022WR034203

Time Series of Electrical Conductivity Fluctuations Give Insights Into Long-Term Solute Transport Dynamics of an Urban Stream

Anna Jaeger[1,2], Jonas L. Schaper[1,3], Paul Romeijn[4], Andrea Betterle[5,6], Malte Posselt[7], Stefan Krause[4,8], Jörg Lewandowski[1,2], and Joakim Riml[9]

[1]Department Ecohydrology and Biogeochemistry, Leibniz Institute of Freshwater Ecology and Inland Fisheries, Berlin, Germany, [2]Geography Department, Humboldt University Berlin, Berlin, Germany, [3]Center for Applied Geoscience, Eberhard Karls University of Tübingen, Tübingen, Germany, [4]School of Geography, Earth and Environmental Sciences, University of Birmingham, Birmingham, UK, [5]European Commission, Joint Research Centre, Ispra, Italy, [6]Eawag, Swiss Federal Institute of Aquatic Science and Technology, Dübendorf, Switzerland, [7]Department of Environmental Science, Stockholm University, Stockholm, Sweden, [8]CNRS, ENTPE, UMR5023, Ecologie des Hydrosystèmes Naturels et Anthropisés (LEHNA), University Lyon, Université Claude Bernard Lyon 1, Villeurbanne, France, [9]Department of Sustainable Development, Environmental Science and Engineering, Royal Institute of Technology, Stockholm, Sweden

Key Points:

- Electrical conductivity fluctuations caused by discharge of treated wastewater into a river contain information about solute transport
- A solute transport model applied to recordings of solute fluctuations can be used to obtain long-term time series of transport metrics
- Differences in transport metrics in adjacent river sections were found; Mowing of macrophytes may increase the transient storage area

Supporting Information:

Supporting Information may be found in the online version of this article.

Correspondence to:

J. Lewandowski,
lewe@igb-berlin.de

Citation:

Jaeger, A., Schaper, J. L., Romeijn, P., Betterle, A., Posselt, M., Krause, S., et al. (2023). Time series of electrical conductivity fluctuations give insights into long-term solute transport dynamics of an urban stream. *Water Resources Research*, *59*, e2022WR034203. https://doi.org/10.1029/2022WR034203

Received 28 NOV 2022
Accepted 1 JUN 2023

© 2023. The Authors.
This is an open access article under the terms of the Creative Commons Attribution-NonCommercial-NoDerivs License, which permits use and distribution in any medium, provided the original work is properly cited, the use is non-commercial and no modifications or adaptations are made.

Abstract Artificial tracers are often used for quantitative estimates of solute transport properties in rivers. However, single-injection tracer tests give insights in transport characteristics limited to the ecohydrological conditions at the testing time. Series of time-consuming and laborious tracer tests would be required to properly capture seasonal changes. The present study uses intrinsic diurnal fluctuations of electrical conductivity (EC) caused by discharge of treated wastewater as a tracer to evaluate solute transport processes along a 4.7-km reach of the River Erpe, Germany. By reproducing the fluctuations recorded along the river using the solute transport model one-dimensional transport with inflow and storage, this study investigated the long-term dynamics in solute transport properties. Individual 48-hr curves of EC were used in the steady state configuration of the model to gain 48-hr-integrated estimates of selected transport parameters. Using a sliding window approach in 1-hr steps along the 2,270-hr time series of EC the temporal variability of solute transport between April and June 2016 was assessed. To test the identifiability of parameters using the proposed method, sensitivity analyses and a breakthrough curve analysis of selected 48-hr windows were implemented. With time advancing into the summer, a significant rising trend (Mann-Kendall test p-value < 0.05) of the cross sectional area of the channel was observed and attributed to the growth of macrophytes and a significant slightly decreasing trend for the storage rate was found. The presented method is of high value for river management, as promoting transient storage enhances biogeochemical cycling and benefits water quality.

1. Introduction

Tracing solute transport is fundamental to improve the understanding of hydrodynamic, chemical and biological processes in rivers and their catchments. In particular, understanding the solute exchange between the main stream channel and retention zones with increased biochemical activity are of high importance to comprehend stream ecosystem mechanisms (Bencala, 1983). The transient storage concept combines all areas of stagnant flow where residence times are higher than in the main channel into a lumped compartment called the transient storage zone. It includes for example, the hyporheic zone, stillwater, zones behind obstacles and vegetation and near-shore pools. These zones can be hotspots of metabolic activity, they play a crucial role for a river's capacity of nutrient retention and removal of micropollutants and provide diverse habitats for aquatic organisms (Blaen et al., 2018; Boano et al., 2014; Kurz et al., 2017; Lewandowski et al., 2019; Peralta-Maraver et al., 2018). A common methodology to estimate solute transport and transient storage behavior is to inject a tracer substance, such as a fluorescent dye, in the stream and measure its breakthrough curve at several points downstream of the injection point. The shape and timing of the breakthrough curve holds information on solute transport that can be interpreted by means of mathematical models. Specifically, these models are useful because they link the model parameters representing key transport characteristics to the observed breakthrough curves of the traced substance (Marion et al., 2003; Wörman, 2000). The transient storage model developed by Bencala and Walters in 1983 is among the most popular tools to describe solute transport along a stream (Bencala & Walters, 1983). In its

simplest form, the model comprises equations accounting for transport in a one-dimensional stream channel and exchange with a single, homogenous transient storage zone.

A major drawback of tracer tests is their requirement for extensive resources, such as considerable amounts of tracer substance and workforce (Kilpatrick et al., 1989). In the end, a single injection solely characterize the solute transport within the timeframe of the test. However, transport behavior is expected to experience temporal variation especially with changing seasonal conditions, such as discharge dynamics and vegetation growth (Kurz et al., 2017; Salehin et al., 2003). Harvey et al. (2003) examined the change in hydraulic retention in a study analyzing annual stream tracer tests over 5 years in a high-gradient perennial desert stream in Arizona. Within the 5 years presence of macrophytes was expanding, streamflow decreased and channel width increased. These changes in stream characteristics were drastic enough that they could be related to a change in transport parameters obtained from five tracer injections. However, often long-term variation and distribution of transport parameters cannot be captured with traditional tracer injections because a larger amount of observations is necessary to monitor gradual changes and multiple repetitions of tracer injections are costly and time-consuming (Ward et al., 2019).

A low-effort method to obtain time series estimates of solute transport and particularly transient storage time series would be of great interest for river management. It would provide insights into changing river conditions throughout the year and facilitate the planning and reviewing of restoration projects, streamflow regulations and overall river ecosystem management. As transient storage enhances biochemical activity, nutrient and contaminant removal and benefits the aquatic community, it is a crucial parameter for river restauration, management and decision making to be assessed on longer time-scales (Lewandowski et al., 2019).

For long-term studies usage of intrinsic concentration time series, meaning concentration changes of suitable solutes already present in the stream, as opposed to artificially created signals would be ideal for estimation of transport parameters. Sometimes those solutes are referred to as "natural" or "environmental" tracers. Here we use the term "intrinsic" as the electrical conductivity (EC) signal used in the present study derives from a wastewater treatment plant (WWTP) and is thus not "naturally" present.

Previously, some studies made use of intrinsic concentration fluctuations for estimation of solute transport in rivers: Ryan et al. (2004) used a fluctuating bromide concentration deriving from groundwater inflow from an abandoned mineral processing plant in a stream in Pennsylvania to assess the solute transport over a 7.5 km reach within 24 hr. In a river bank filtration setting, fluctuations of EC and a deconvolution method were used to calculate the solute transport from a river in Switzerland to a well over a period of 2 years (Cirpka et al., 2007; Vogt et al., 2010). A similar study was conducted in Ohio using a cross-correlation method to estimate travel times from the river to nearby wells (Sheets et al., 2002). Hyporheic travel times within different locations of an in-stream gravel bar were estimated using EC variations over a study period of more than a month (Schmidt et al., 2012). Two studies at rivers that receive treated wastewater in Southwestern Germany used EC fluctuations to calculate the transit time distributions as basis for determination of micropollutant attenuation (Glaser et al., 2020; Schwientek et al., 2016). In River Erpe located in Berlin/Brandenburg, Germany, the river investigated in the present study, previously EC fluctuations were used to calculate solute transport within the sediment using the advection-dispersion equation and to estimate travel times in the surface water by deconvolution of EC signals over a 4-day period (Jaeger et al., 2019; Schaper et al., 2019). However, to the best of our knowledge no study was previously conducted to quantify seasonal dynamics of transport properties in streams from intrinsic concentration fluctuations over an extended study period.

In the present study we analyzed long-term EC fluctuations (spanning months) as an intrinsic tracer for solute transport dynamics in the surface water of the River Erpe. The River Erpe is a stream that receives regularly fluctuating discharge of treated wastewater, resulting in characteristic daily fluctuations of solute concentrations. We used hourly consecutive 48-hr windows of EC signals as breakthrough curves for steady-state simulations using the parameter estimation function of the solute transport model program "One-dimensional transport with inflow and storage" (OTIS) (Runkel, 1998).

OTIS was designed to make solute transport modeling easily accessible and user-friendly even for practitioners without detailed expertise in solute transport modeling (Runkel, 1998). The approach developed in the present study is suggested to be generally applicable to readily estimate solute transport time series in streams which receive WWTP effluents or any inflow characterized by a regular EC fluctuation, because neither measurements of EC time series nor application of OTIS require costly resources or specialist expertise.

19447973, 2023, 7, Downloaded from https://agupubs.onlinelibrary.wiley.com/doi/10.1029/2022WR034203 by Paul Scherrer Institut PSI, Wiley Online Library on [20/07/2023]. See the Terms and Conditions (https://onlinelibrary.wiley.com/terms-and-conditions) on Wiley Online Library for rules of use; OA articles are governed by the applicable Creative Commons License

19447973, 2023, 7, Downloaded from https://agupubs.onlinelibrary.wiley.com/doi/10.1029/2022WR034203 by Paul Scherrer Institut PSI, Wiley Online Library on [20/07/2023]. See the Terms and Conditions (https://onlinelibrary.wiley.com/terms-and-conditions) on Wiley Online Library for rules of use; OA articles are governed by the applicable Creative Commons License

The 48-hr EC curves deviate from the breakthrough curves of traditional slug injections, in particular with regards to the lack of distinct tailing behavior. The slope of the tail of the breakthrough curve of a tracer slug injection can provide valuable insights into the longer exchange flow paths between river and transient storage zones and is important for characterizing residence time distributions in streambed sediments or in-stream vegetation (Haggerty et al., 2002; Wörman et al., 2002). The signal is less favorable for many natural tracers when such information can be partly masked by a continuous strong stream signal in the case of intrinsic reoccurring fluctuations. Yet despite the absence of a pronounced tail, assessment of continuous time series of solute concentration might still contain vital information on the transient storage behavior. We investigated this by assessing the performance of the transient storage model constrained by intrinsic EC fluctuations by means of a Monte Carlo sensitivity analysis, a Sobol sensitivity analysis, an analysis which describes how variability in model parameters influence the variability in model output, and a breakthrough curve analysis. The signal complexity of observed EC time series might have advantages to traditional slug injections and help distinguishing between dispersion and transient storage parameters. We also discuss the impact of fluctuating discharge on the model performance and compare the results of the parameter estimation using the EC time series with results of a traditional slug injection. Finally, we compare results from two adjacent stream sections (Sections 1 and 2) of a 4.7 km reach, as well as the impact of macrophyte removal of Section 1 on the solute transport parameters.

The aim of the study is to assess whether time-varying solute transport parameters including transient storage metrics can be estimated by fitting solutions of the one-dimensional steady transport model to daily fluctuations in EC and thereby obtain a time series of transport parameters extending a period of several months. We furthermore hypothesize to observe a rise in the transient storage zone area and related transient storage metrics within the study time from April to July 2016 due to the growth of macrophytes along the reach. We expect to see general differences in the distributions of the transport model parameters in the two sections of the reach due to their different geomorphological characteristics. Specifically, in Section 1, the first 1.6 km stretch of the study reach, we generally expect higher transient storage due to the presence of fish ladders, higher presence of macrophytes, a side channel and more conductive streambed sediment compared to Section 2, the adjacent 3.1 km stretch of the study reach. Finally, we expect to encounter considerable differences in transient storage before and after macrophytes are removed from Section 1.

2. Methods

2.1. Site Description

The River Erpe is an urban lowland stream in the east of Berlin and originates in the federal state Brandenburg, Germany. It is heavily impacted by the discharge of a major wastewater treatment plant (WWTP, 300,000 PE) roughly 7 km upstream of its outlet into the River Spree (Figure 1). The river has previously been subject to various multi-scale investigations reaching from cm to reach-scale field investigations (Jaeger et al., 2019; Mechelke et al., 2019; Peralta-Maraver et al., 2018; Posselt et al., 2018; Schaper et al., 2019). The study reach of 4.7 km length starts 0.7 km after the inflow of treated wastewater and is divided into Section 1 (1.6 km length) and Section 2 (3.1 km length). The study reach has been described in detail in Jaeger et al. (2019). Section 1 contains stretches, where the stream water infiltrates into the riparian groundwater (Schaper et al., 2019). In Section 2 the streambed is confined by muddy sediment and has no connection to the aquifer (Jaeger et al., 2019). Due to the high portion of treated wastewater (60%–80%) the river carries high nutrient loads leading to substantial growth of macrophytes in summer, especially in non-shaded areas. The river is channelized with a width of roughly 9 m and mostly steep riverbanks. In Section 1, a side channel diverts and re-enters the main channel. In addition, two fish ladders are located in Section 1. While Section 1 is located in a nature conservation area and only 5% of its channel is shaded by canopy, Section 2 is located in a residential area and roughly 58% of its channel is shaded by canopy. Therefore, abundance of submerged macrophytes in summer is considerably higher in Section 1 than in Section 2. In June 2016 a dry biomass of 176 ± 87.3 g m^{-2} was measured for Section 1 and a dry biomass of $\sim$78 g m^{-2} was estimated for Section 2 (Jaeger et al., 2019). To avoid the risk of flooding, the channel of River Erpe is cleared from macrophytes seasonally (also termed "mowing"). During the time period investigated in the present study Section 1 was mowed on 17 June 2016 (Figure 1). The plants were cut by trucks with attached mowing shovels, removed from the water and piled on the shore (see Figure S2 of the Supporting Information of Jaeger et al., 2019).

2.2. Field Measurements

A major characteristic of the River Erpe are the daily fluctuations in solutes and discharge deriving from the regularly fluctuating inflow volume of treated wastewater (Jaeger et al., 2019; Peralta-Maraver et al., 2018;

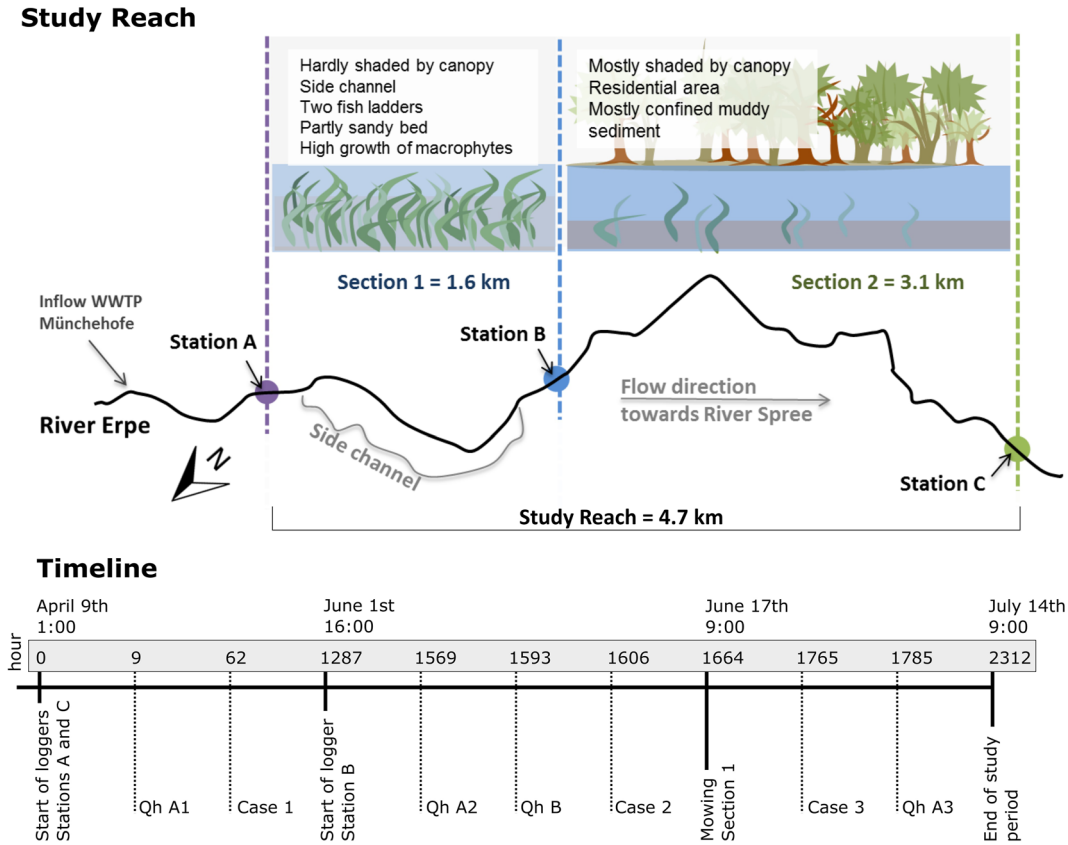

Figure 1. Study reach along the River Erpe and timeline of the experiment. Section 1 is located between stations A and B, Section 2 is located between stations B and C. The study period starts 9 April 2016 1:00 (denoted hour 0) and ends 14 July 2016 9:00 (denoted hour 2,312). Cases 1–3 indicate start times of example cases of 48-hr time windows used for the sensitivity analysis. Qh A1–3 and Qh B indicate start times of recording of discharge (Q)—water level (h) relationships at stations A and B, respectively. Note that the timeline is not to scale. Figure adapted from Jaeger et al. (2019), further permission for reuse of the Figure should be directed to the American Chemical Society.

Schaper et al., 2019). To capture these fluctuations we installed data loggers measuring EC, water pressure and water temperature at three locations: Station A (start of study reach), Station B (1.6 km downstream of A) and Station C (end of study reach, 4.7 km downstream of A; Figure 1). In the present study we investigate 15-min-interval data from April (9 April 2016 1:00; denoted hour 0) to July (14 July 2016 9:00; denoted hour 2,312). The logger data outliers and missing values (Station A: 0.3%; Station B: 0.02%; Station C: 0.05%; maximum gap: 9 values [2:15 hr]) were replaced with values obtained by linear interpolation. Air temperature, precipitation and air pressure were recorded by a weather station in the vicinity (2.6 km southeast of sampling station B, IGB Berlin).

Power-law rating curves at the gauging stations (denoted Qh) were established by associating streamflow measurements with the corresponding water stage (derived from pressure records) for different flow conditions. Direct streamflow measurements were obtained using a handheld electromagnetic water flow meter (OTT MF Pro, OTT HydroMet, Kempten, Germany) in April and an Acoustic Doppler Current Profiler (StreamPro ADCP by Teledyne RD Instruments, La Gaude, France) in June. We conducted measurements three times at Station A (Qh A1: 9 April 2016; Qh A2: 13 June 2016; Qh A3: 22 June 2016) and one time at Station B (Qh B: 14 June 2016). Due to the growth of macrophytes and other seasonal changes, the discharge (Q)—water stage (h) relation changes over time. Hence, we calculated the discharge at Station A before macrophyte removal of Section 1 (hour 0 to hour 1,663), using a share of Qh A1 and Qh A2 by linearly increasing the share of Qh A2 from 0% to 100%. The discharge of the time after macrophyte removal was calculated using Qh A3, as this was most representative for the conditions in the time after macrophyte removal of Section 1. For the discharge calculation in Station B (only hours 1,287–2,300), we used Qh B (Figure S1 in Supporting Information S1).

19447973, 2023, 7, Downloaded from https://agupubs.onlinelibrary.wiley.com/doi/10.1029/2022WR034203 by Paul Scherrer Institut PSI, Wiley Online Library on [20/07/2023]. See the Terms and Conditions (https://onlinelibrary.wiley.com/terms-and-conditions) on Wiley Online Library for rules of use; OA articles are governed by the applicable Creative Commons License

19447973, 2023, 7, Downloaded from https://agupubs.onlinelibrary.wiley.com/doi/10.1029/2022WR034203 by Paul Scherrer Institut PSI, Wiley Online Library on [20/07/2023]. See the Terms and Conditions (https://onlinelibrary.wiley.com/terms-and-conditions) on Wiley Online Library for rules of use; OA articles are governed by the applicable Creative Commons License

Three example cases of 48-hr time windows are used in the present study to evaluate the performance of the EC curves, denoted Cases 1–3 starting at hours 62, 1,606, and 1,765, respectively. The three cases correspond to 48-hr water-sampling times at Stations A, B, and C reported in related studies by Posselt et al. (2018) (Case 1) and Jaeger et al. (2019) (Cases 2 and 3).

2.3. The 1D Solute Transport Equation

The 1D transport model is based on a set of equations that describe the solute advection, dispersion and transient storage developed by Bencala and Walters (1983) (Bencala, 1983; Runkel, 1998). It accounts for two conceptual areas within a stream, namely the main channel and the transient storage zone, and the solute transport within and between them. In its simplest version the transient storage zone is a lumped system, which consists of zones of stagnant flow, for example, in hyporheic zones, pools, eddies and areas around vegetation. The conservative longitudinal solute transport and the interaction between the main channel and the lumped storage zones is described by the advection-dispersion equation together with an exchange flux between the main channel and the storage zone according to:

$$\frac{\partial C}{\partial t} = -\frac{Q\partial C}{A\partial x} + \frac{\partial}{A\partial x}\left(\mathrm{AD}\frac{\partial C}{\partial x}\right) + \frac{q_{\mathrm{LIN}}}{A}(C_L - C) + \alpha(C_S - C) \quad (1)$$

$$\frac{\partial C_S}{\partial t} = \alpha\frac{A}{A_S}(C_S - C) \quad (2)$$

A (m^2) is the cross-sectional area of the main channel, A_S (m^2) is the storage zone cross-sectional area, C (mS cm^{-1}) is the main channel solute concentration, C_L (mS cm^{-1}) is the lateral inflow solute concentration, C_S (mS cm^{-1}) is the storage zone solute concentration, D (m^2 s^{-1}) is the dispersion coefficient, Q (m^3 s^{-1}) is the discharge, q_{LIN} (m^2 s^{-1}) is the lateral inflow rate per stream length and α (s^{-1}) is the storage zone exchange rate. In the present case q_{LIN} is assumed negligible and thus set to 0.

2.4. OTIS Implementation and Settings

In the OTIS programs, Equations 1 and 2 are solved using a Crank-Nicolson scheme for finite-differences approximating the spatial derivatives. For more details on the solution schemes, we refer to Runkel (1998). The original OTIS program calculates a concentration curve at the downstream station based on the solute concentration time series at the upstream station (i.e., the pre-defined boundary condition) and given transport parameters (A, A_S, D, α and Q). The OTIS-P program, in turn, estimates the solute transport parameters given two concentration curves at different measurement stations via nonlinear least square optimization based on the NL2SOL software package, that minimizes the residual sum of squares (RSS) using an iterative procedure (Dennis et al., 1981). The OTIS-P results aim to converge toward minimal change in estimated values or a minimal change in model performance.

For conservative, steady-state calculations OTIS mainly requires the time-varying boundary condition, a start time (TSTART), an end time (TFINAL) and a set of transport parameters. For the present work, EC fluctuations within 48 hr were analyzed under a steady-state assumption. The EC fluctuations in River Erpe reoccur every 24 hr, but 24-hr time windows proved not to be sufficiently long to achieve stable results. The best model performances were obtained using a 48-hr window featuring two daily troughs in the WWTP effluent EC signal (e.g., Figure 2, p5). Hence, the model was always run from TSTART to TFINAL, where TFINAL was TSTART + 48 hr. EC concentrations at the starting station (A or B) at 15 min intervals from TSTART to TFINAL + 2 hr were used as boundary conditions. Two hours were added to TFINAL because the model requires the upstream concentration series to exceed TFINAL. An interval of 15 min (every third observation) was used to reduce the calculation time of the model. The discharge (Q_{av}) for a given window was calculated by averaging the discharge at the upstream station from TSTART to TFINAL. The average of Q_{av} of all 48-hr windows was 0.47 m^3 s^{-1} and varied within 48 hr on average from 0.68 m^3 s^{-1} (90th percentile) to 0.24 m^3 s^{-1} (10th percentile) (Figure S2 in Supporting Information S1). Depending on the type of analysis conducted in the present study, different initial conditions of A, A_S, D and α were set. For the OTIS-P parameter estimations additionally observed downstream concentration curves were used to calibrate the model parameters. The average advective travel time ($t_{\mathrm{adv\_estim}}$) between Stations A and C was estimated on the basis of the daily trough-transit-time and found to be roughly 8 hr, in Sections 1 and 2 it was assumed to be roughly 4 hr each. So, in order to approximately capture the same parcel downstream,

10.1029/2022WR034203

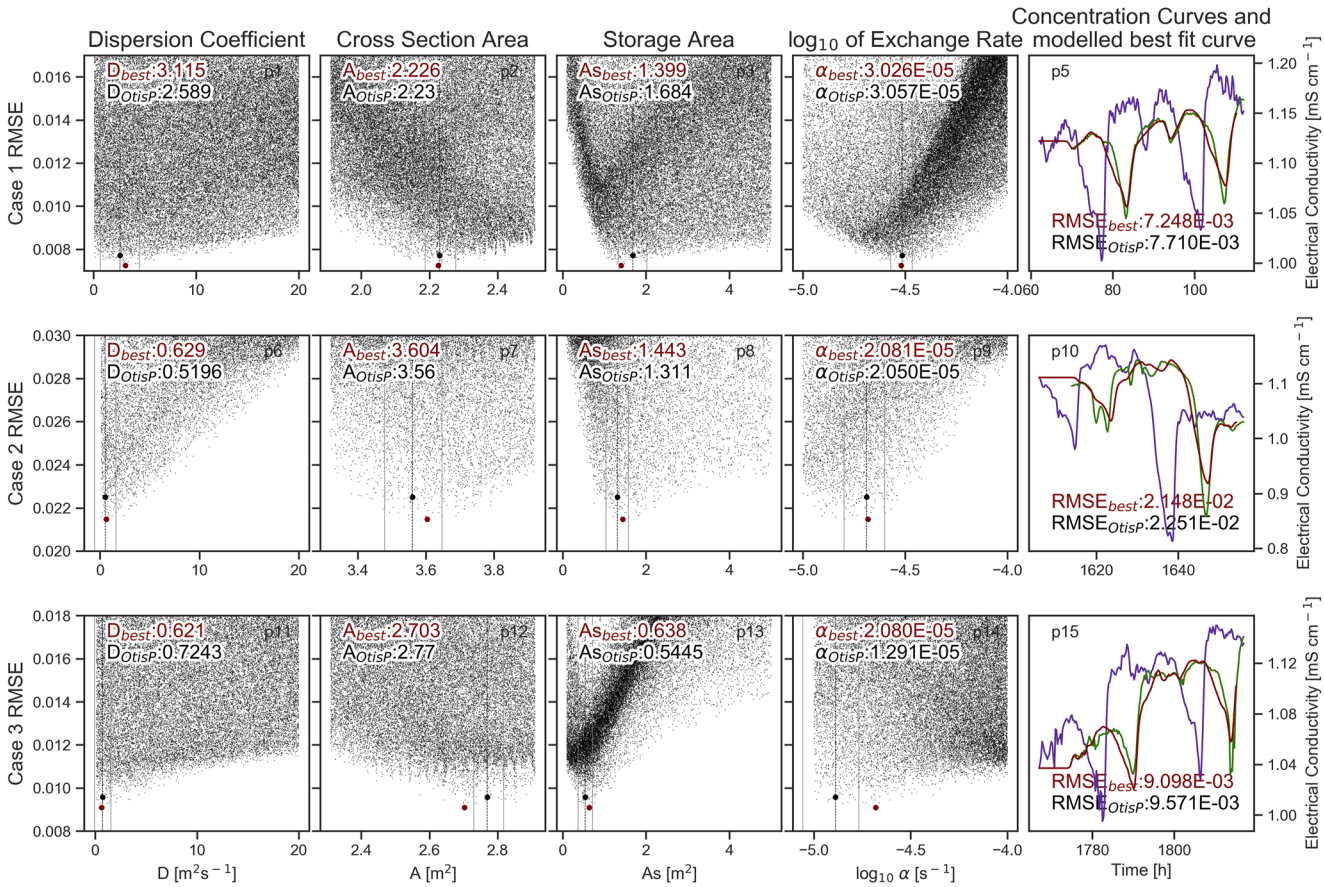

Figure 2. Sensitivity analyses (Suites 3) of one-dimensional transport with inflow and storage models of three 48-hr windows starting from hour 62 (Case 1), hour 1,606 (Case 2) and hour 1,765 (Case 3), respectively. The scatterplots to the left show model results of the randomly selected parameter sets (D, A, A_S, and α) and resulting goodness of fit (Root mean squared error [RMSE]) of the modeled (red line) to the measured electrical conductivity (EC) curves (green lines in plots p5, p10, and p15 on the right). The red points in the scatter plots indicate the parameter set of the "best" fits (lowest RMSE). The black markers indicate the results obtained from the OTIS-P parameter estimation. The gray lines show the respective upper and lower limits of the 95% confidence intervals of the OTIS-P fitting. The red lines in p5, p10, and p15 depict the curve of "best" fit (lowest RMSE) to the measured EC curves at the downstream Station C (green line). The concentrations at the upstream Station A used as upstream boundary conditions are shown in purple. Note the differences in scales of RMSE and the parameters.

the downstream concentration curve started TSTART + t_{adv_estim} and ended TFINAL + t_{adv_estim} + 2. Additionally, a data-correction routine was implemented due to shifts in EC records over long-time measurements (presumably caused by biofilm growth on the sensors). We assumed no dilution along the reach, because to the best of our knowledge there is no external lateral inflow. A discharge mass balance was not calculated, as the river is a losing stream in Section 1 (Schaper et al., 2018) and, therefore, a large portion of lateral outflow is unknown. The maximum amount of rain was 15 mm per hour and for only 1% of the time direct dilution by rain falling on the channel was higher than 0.5% (Figure S2 in Supporting Information S1). Hence, direct dilution of the river water by rain was negligible (rising discharge during rain events results from higher amounts of treated wastewater discharging into the river prior to Station A). Therefore, for the correction routine, the downstream EC curve was automatically shifted in order to match the 50-hr average of the upstream EC records.

The appropriate selection of the spatial and numerical resolution ensures the stability of the solutions to the differential equation in solute transport simulations. The criterion adopted in this study is the Courant-Friedrichs-Lewy condition (Courant et al., 1928): a relationship between flow velocity ($u = Q_{av}/A$) to the ratio of the spatial (Δx) and temporal (Δt) discretization (Courant et al., 1928). If $u/(\Delta x/\Delta t)$ exceeds 1, the solution is deemed unstable. Therefore, Δx was set to 20 m and Δt was adapted to the criterion variably for each run (sensitivity analyses) or low enough (0.02 hr), so the majority of the runs met the criterion (time series analysis).

For comparability with the sensitivity analysis, the RSS returned by OTIS-P was converted to the root-mean-square-error (RMSE, Equation 3). In this work we generally refer to the RMSE as the criteria for the goodness of fit.

19447973, 2023, 7, Downloaded from https://agupubs.onlinelibrary.wiley.com/doi/10.1029/2022WR034203 by Paul Scherrer Institut PSI, Wiley Online Library on [20/07/2023]. See the Terms and Conditions (https://onlinelibrary.wiley.com/terms-and-conditions) on Wiley Online Library for rules of use; OA articles are governed by the applicable Creative Commons License

$$\mathrm{RMSE} = \sqrt{\frac{1}{n}\sum_{k=1}^{n}(O_k - S_k)^2} \quad (3)$$

O_k are the measured EC values and S_k are the corresponding OTIS-P simulations at each time step k; n is the number of times steps.

In addition to the RSS and the estimated values, the OTIS-P package provides confidence intervals calculated within the neighborhood of the estimated parameters. Those statistics are based on the variance-covariance matrix for the solutions calculated by the nonlinear least squares algorithm (Donaldson & Tryon, 1987; Kelleher et al., 2013). However, these values are not representative for the global behavior of the parameters on the feasible parameter space (Kelleher et al., 2013; Ward et al., 2017).

A set of text files serves as the user interface for input settings and an executable file runs the program that returns text files as output. We developed a program that automatically writes inputs, runs the program and reads the outputs using Python 3 (Van Rossum & Drake, 2003). This way we were able to repeatedly run large amounts of simulations and easily capture the distribution of results.

2.5. Sensitivity Analyses

Optimization algorithms applied to inverse models such as OTIS-P are a quick method that provides a single set of estimated parameters based on the predefined objection function. However, initial parameter values may lead to convergence toward local minima and the procedure lacks information about the global sensitivity in model output to uncertainties in the model parameters (Kelleher et al., 2013; Riml et al., 2013; Ward et al., 2017). Ward et al. (2017) argue that the confidence intervals calculated by OTIS-P do not suffice the high uncertainty of transient storage estimates inherent in solute tracer tests, and suggest using Monte Carlo analyses to cover a wider parameter space and obtain a meaningful analysis of the sensitivity of the model parameters.

We therefore implemented OTIS in a program, that randomly drew parameter sets (A, A_S, D and α) out of given prior ranges of uniform distributions and returned the RMSE between the calculated model output and the measured solute concentrations resulting from each parameter set. To meet the stability criterion of the numerical solutions even at very low values of A, Δt was reset dependent on A in every run, so that the Courant-Friedrichs-Lewy condition equaled 0.5.

We used the 48-hr windows for Case 1 (TSTART hour 62), Case 2 (TSTART hour 1,606) and Case 3 (TSTART hour 1,765) to assess the parameter sensitivities, following an approach similar to the Monte Carlo analysis tool established by Ward et al. (2017). Starting at a wide parameter range, we reduced the ranges in three steps (denoted Suites 1–3) toward the best performing parameter sets (minimum RMSE). As A is usually the parameter the model is most sensitive to, the prior range of A was narrowed down initially (Suite 1). We estimated A_{estim} from the estimated flow velocity (u) using the "peak transit time," which in this case can be better described as the "trough transit time," (i.e., the time difference between two consecutive troughs of the EC signal) and the average discharge Q_{av} within the 48 hr (April: 2.17 m^2; June before mowing: 5.29 m^2; June after mowing: 3.80 m^2). We performed 10,000 simulations using a wide prior range of $A_{\mathrm{estim}} \pm 2$ m^2 while the other parameter ranges were chosen based on our previous experience from values estimated by OTIS-P (D: 0.1–30 $m^2 s^{-1}$; A_S: 0.1–15 m^2; α: $1 * 10^{-6}$–$1 * 10^{-4}$ s^{-1}). In Suite 2 we narrowed down the range to $A \pm 0.3$ m^2 with A resulting from the best fit of Suite 1 while keeping all the other parameter ranges from Suite 1 and performed another 50,000 simulations (Suite 2). Finally, we narrowed down the prior ranges of D, A_S and α toward the RMSE minimum and performed another 50,000 simulations (Suite 3). The progression of the suites of the three example cases and their respective results are shown in Figures S3–S5 in Supporting Information S1.

To obtain a quantitative measure of the sensitivity of model parameter estimates, we performed a Sobol's sensitivity analysis following the studies of Kelleher et al. (2013) and Riml et al. (2013). Sobol's sensitivity analysis (Sobol, 2001) is a global and model-independent method based on variance decomposition. It divides the total variance in the model output $V(Y)$ into contributions of individual input parameters and parameter interactions. In the present case, the model output Y is the RMSE.

$$S_i = \frac{V_i}{V(Y)} \quad (4)$$

19447973, 2023, 7, Downloaded from https://agupubs.onlinelibrary.wiley.com/doi/10.1029/2022WR034203 by Paul Scherrer Institut PSI, Wiley Online Library on [20/07/2023]. See the Terms and Conditions (https://onlinelibrary.wiley.com/terms-and-conditions) on Wiley Online Library for rules of use; OA articles are governed by the applicable Creative Commons License

$$S_{\mathrm{Ti}} = \frac{V_i + V_{ij} + V_{ijk} + \cdots + V_{12\ldots n}}{V(Y)} \quad (5)$$

The first order index (S_i) is a measure for the variance contribution of each individual input parameter to the model output variance. In other words, if an individual parameter would be fixed, the model output variance would be diminished by the parameter's individual variance contribution (Nossent et al., 2011). The total order index (S_{Ti}) represents the combined variance in output due to a parameter and its interactions with other parameters. Therefore, it is the sum of interaction indices and the first order index.

The sensitivity analysis is dependent on associated parameter ranges. In the present case, similar to the sensitivity analysis after Ward et al. (2017) we calculated the Sobol indices for three example cases (Cases 1–3) in the three respective sets of parameter ranges (Suites 1–3), that were used for the Monte Carlo analysis.

In addition, we run a Sobol analysis using the 5th and the 95th percentiles of parameters obtained in the time-series analysis (whole reach) as parameter ranges. The Python package SALib was used to create the data set of 50,000 runs after Saltelli (2002) and subsequently apply the Sobol analysis.

2.6. Breakthrough Curve Analysis

For the breakthrough curve analysis, the 48-hr window of example Case 1 (TSTART hour 62) was used. While one parameter (A_S, D and α, respectively) was varied randomly 500 times within a given range (D: 0–30 m^2s^{-1}, A_S: 0–5 m^2, α: 10^{-6}–10^{-4} s^{-1}), the remaining three parameters were fixed to the results of the best fits of Suite 3 of the sensitivity analysis (Figure 2). This way the individual influences of the three parameters on the breakthrough curves were illustrated. A second set of runs under the same conditions was executed, but this time an artificial boundary concentration curve was given as input. This curve is imitating the shape of a conventional slug injection.

2.7. Comparison to Tracer Test Data

In June 2016 several slug injections of a fluorescent tracer were performed in River Erpe along Section 1. The detailed methods and analysis of the tracer tests are described in Romeijn et al. (2021). For the purpose of the present study, we aimed to use two of the slug tests (Injection 1 starting at hour 1,640 [before mowing] and Injection 2 starting at hour 1,760 [after mowing]) to compare the resulting parameter estimates to the results of the time series analysis of EC curves. Approximately 25 g of fluorescein were dissolved in 10 L of stream water and released into the river across the width of the channel aiming to reach a concentration of 33 µg L^{-1} in the river. The injection point was close to the confluence of the river and the treated wastewater, roughly 700 m upstream of Station A. High-frequency online fluorometers (Albillia Sarl GGUN FL30 field fluorometers, Neuchatel, CH) were located at stations A and B on a frame on top of the riverbed to record the tracer concentrations at 10 s intervals. Due to detection limits, the tracer breakthrough curves had to be truncated below 0.1 µg L^{-1} leading to a tracer-curve duration of roughly 8 hr. The tracer curves were implemented in OTIS-P for estimation of the transport parameters as described above. Due to non-convergence of the OTIS-P results, additionally a Monte Carlo sensitivity analysis as described above was conducted for both tracer injection events. To be able to compare the calculated tracer curves based on the parameters estimated in the EC-time series to the measured curves, all parameter estimates of 48-hr windows that comprised the 8-hr time-span were used. Results that did not converge or featured outliers ($A > 10$ m^2, $A_S > 10$ m^2, $D > 20$ m^2 s^{-1}, $\alpha > 10^{-4}$) were excluded. Therefore, out of 24 parameter sets 16 and 24 were used to simulate curves to be compared to the measured breakthrough of Injection 1 and 2, respectively.

2.8. Time Series Analysis

The EC time series was analyzed using OTIS-P under the settings described above. A program was set up that consecutively analyzed 48-hr windows in 1-hr time steps. Each window is identified by its starting hour (TSTART). Generally, if a model run did not converge, the simulation was repeated using the output parameters of the previous run as initial parameters of the next run for a maximum of 15 times. If the 15th run did not converge, the initial parameters were set back to a set of parameters ($D = 1.0$, $A = 2.6$, $A_S = 1.1$, $\alpha = 2.1 * 10^{-5}$) which were median values of parameter results of the whole timespan in preliminary analyses. If the simulation

19447973, 2023, 7, Downloaded from https://agupubs.onlinelibrary.wiley.com/doi/10.1029/2022WR034203 by Paul Scherrer Institut PSI, Wiley Online Library on [20/07/2023]. See the Terms and Conditions (https://onlinelibrary.wiley.com/terms-and-conditions) on Wiley Online Library for rules of use; OA articles are governed by the applicable Creative Commons License

19447973, 2023, 7, Downloaded from https://agupubs.onlinelibrary.wiley.com/doi/10.1029/2022WR034203 by Paul Scherrer Institut PSI, Wiley Online Library on [20/07/2023]. See the Terms and Conditions (https://onlinelibrary.wiley.com/terms-and-conditions) on Wiley Online Library for rules of use; OA articles are governed by the applicable Creative Commons License

still did not converge 15 more runs after the setback to the median parameters, the window was marked as "no solution" and the program moved on to the next window. As soon as a run converged, the output parameters were saved and the program moved on to the next window. For the next window, the output parameters of the last previous window that converged and that complied with the criteria $D < 50\ m^2\ s^{-1}$, $A_S < 50\ m^2$ and $\alpha < 10\ s^{-1}$ were used as start parameters. These criteria were set to avoid an unreasonable upwards-spiral of parameters, which could result in repeated cases of non-convergence of windows that would normally converge at lower start values. Δt was set to 0.02 hr, which results in Courant-Friedrichs-Lewy conditions of <1 for the majority of 48-hr windows. If the resulting estimated parameters of 48-hr windows did not meet the criterion, they were accounted among the "no solution" runs.

To detect trends in the time series of the parameter estimates, a non-parametric Mann-Kendall test was a applied and a Sen's slope estimator was calculated for daily median parameter values ($n = 97$). Prior to analysis, parameter estimates above the 99th percentile of the hourly values were removed. The significance level (p) was set to 5%.

For the analysis of Sections 1 and 2 (starting hour 1,287), the same iteration scheme as for the reach-scale analysis was used. In Section 1 boundary conditions were EC curves from Station A and downstream observations were EC curves from Station B. In Section 2 boundary conditions were EC curves from Station B and downstream observations were EC curves from Station C. The initial values of the first runs of the first windows to which the parameters were set back to after the 15th run of non-convergence were median values of preliminary analyses (Section 1: $D = 0.8\ m^2\ s^{-1}$, $A = 3.7\ m^2$, $A_S = 2.7\ m^2$, $\alpha = 3.3 * 10^{-5}\ s^{-1}$; Section 2: $D = 2.7\ m^2\ s^{-1}$, $A = 2.4\ m^2$, $A_S = 0.8\ m^2$, $\alpha = 1.1 * 10^{-5}\ s^{-1}$).

For interpretation of the changes in solute transport, the transient storage metrics F_{med} and the Damköhler number DaI as well as the advective travel time t_{adv} were calculated from the parameter estimates. The t_{adv} (s) is the reach length L (m) divided by the advective velocity u ($m\ s^{-1}$), which is calculated as the quotient of Q_{av} and A. F_{med} is a transient storage metric that represents the portion of median travel time that is caused by transient storage defined as (Runkel, 2002):

$$F_{med} \cong \left(1 - e^{-L(\alpha/u)}\right) * \frac{A_S}{A + A_S} \tag{6}$$

DaI represents the ratio of t_{adv} to the transient storage zone interaction timescale, which potentially provides information about the dominating time scale controlling solute transport. DaI is defined as (Bahr & Rubin, 1987; Kelleher et al., 2013):

$$\mathrm{DaI} = \alpha\left(1 + \frac{A}{A_S}\right) * \frac{L}{u} \tag{7}$$

In addition, T_{sto} was calculated, which is the storage zone residence time (Runkel, 2002):

$$T_{sto} = \frac{A_S}{\alpha A} \tag{8}$$

3. Results

3.1. Sensitivity Analyses

The consecutive execution of Suites 1–3 led to a stepwise improvement of the best fits (lower RMSE) for all cases (Figure 2). Visually, the modeled best fit curves fit the measured concentrations. Deviations are seen mostly in the areas of the tip of the troughs (Figure 2, panels 5, 10, and 15). In all cases the best fits of Suites 2 and 3 improved the fit of the OTIS-P result, while RMSE of Suites 1 were higher than the OTIS-P results (Figures S3–S5 in Supporting Information S1). Only the best fits of Suites 1 fell outside the 95% confidence interval of the respective results from the parameter fit of OTIS-P in many cases. All the best fits of Suites 3 laid within the 95% confidence interval obtained with OTIS-P, except for the fit of α and A in Case 3 (Figure 2). Within the ranges of Suites 3, all four estimated parameters were converging toward a global minimum. Least identifiable were A and α in Case 3, because here the values do not clearly "dip" toward global minima and are lacking "sharpness," as termed as indicators for sensitivity by Ward et al. (2017).

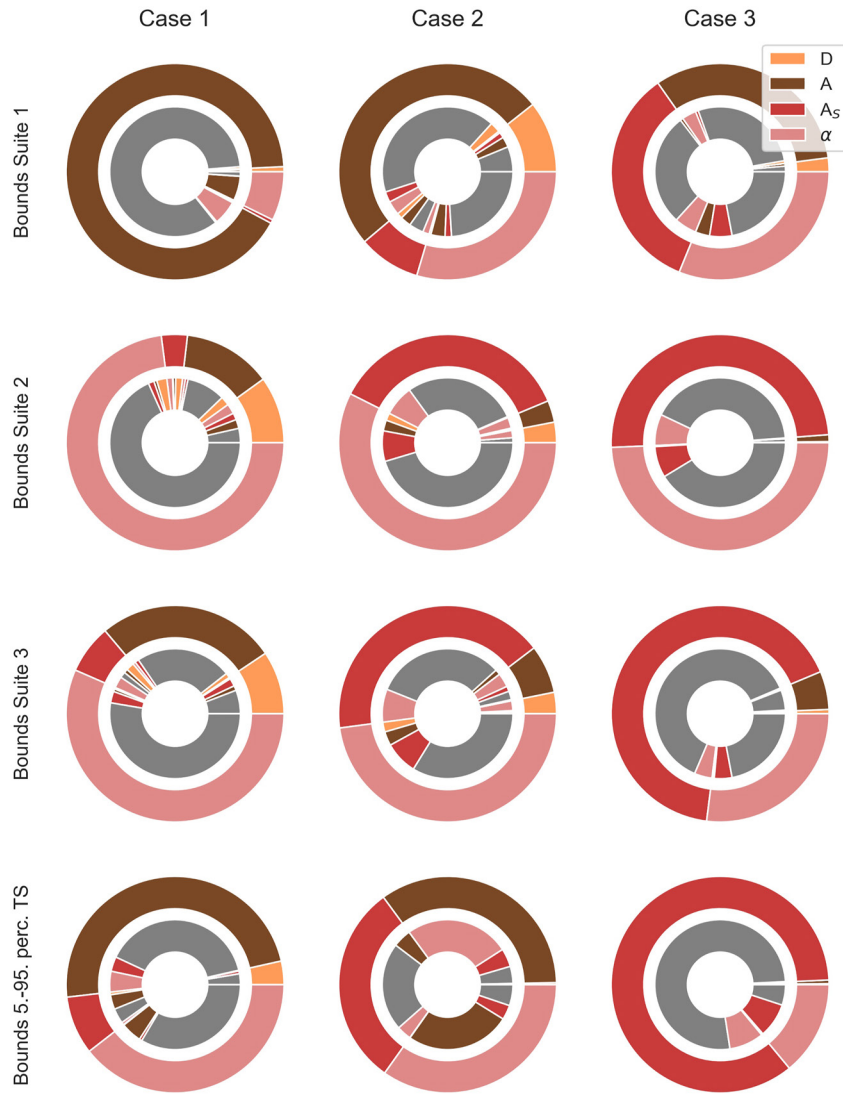

Figure 3. Results of the Sobol sensitivity analysis illustrated in circle-diagrams. Outer rings represent the total order index (S_{Ti}) of each parameter, inner circles depict the first order index (S_i, gray areas) and the interaction indices with the respective other parameters. The first three rows show analyses implemented within the parameter ranges of Suites 1–3 as defined in the Monte Carlo analysis. The last row shows the analyses implemented with boundaries within the 5th and 95th percentiles of parameter distributions obtained in the time series analysis. The illustrations are adapted from Kelleher et al. (2013). Absolute values are shown in Table S2 in Supporting Information S1 and ranges of the analyses in Table S1 in Supporting Information S1.

The results of the Sobol analysis depend considerably on the parameter ranges (Table S1 in Supporting Information S1), which is highlighted in all three example cases, where the first and total order indices changed substantially between the different Suites (Figure 3). This is particularly clearly seen in the change from Suites 1 to 2, where generally the dominance of A in the total order indices is turned to a dominance of α. In Suites 3 the high influence of α dominating the indices in Suites 2 gets reduced, giving more room for relative influence of the other parameters. Other than that, the distributions of total and first-order indices among parameters do not change largely from Suites 2 to Suites 3. Within the ranges of the 5th to the 95th percentiles of the results obtained by the time series analysis, which represent the most relevant boundaries for the 48-hr windows of the present study, the Sobol indices resemble the results of the third Suites. In Case 1 all parameters have relevant influence on the model result, while in Case 2 the influence of D is negligible and the other three parameters have equal shares in total-order indices, where indices of A and α mainly consist of interaction indices with each other. In Case 3, clearly A_S is dominating the model result with a considerable contribution of α.

19447973, 2023, 7, Downloaded from https://agupubs.onlinelibrary.wiley.com/doi/10.1029/2022WR034203 by Paul Scherrer Institut PSI, Wiley Online Library on [20/07/2023]. See the Terms and Conditions (https://onlinelibrary.wiley.com/terms-and-conditions) on Wiley Online Library for rules of use; OA articles are governed by the applicable Creative Commons License

19447973, 2023, 7, Downloaded from https://agupubs.onlinelibrary.wiley.com/doi/10.1029/2022WR034203 by Paul Scherrer Institut PSI, Wiley Online Library on [20/07/2023]. See the Terms and Conditions (https://onlinelibrary.wiley.com/terms-and-conditions) on Wiley Online Library for rules of use; OA articles are governed by the applicable Creative Commons License

Between cases, the highest difference was observed in Case 1, where A_S showed considerably less relative influence on the model output in all Suites compared to Cases 2 and 3. In contrast, in Case 3 the influence of D and A is continuously smaller than in Cases 1 and 2. Overall, depending on Case and set of boundaries, A, A_S and α show high potential for sensitivity, meaning that depending on the specific 48-hr window the parameters are likely to influence the model output. In contrast, the model continuously shows low to no sensitivity to D among the Cases (Figure 3). It has to be emphasized that these are only three out of more than 2,000 48-hr windows and are not meant to represent the conditions in specific times of the studied period, but meant to give an insight into the variability in model output possibilities and sensitivities to model parameter among the set of single 48-hr analyses.

3.2. Breakthrough Curve Analysis

We used the 48-hr window of Case 1 to analyze the effect of variation in dispersion (D) and transient storage parameters (A_S and α) on the shape of the breakthrough curve. As Schmadel et al. (2016) pointed out, the characteristics of a common breakthrough curve caused by a slug injection that may distinguish between the effect of dispersion and transient storage parameters are marginal. However, the shape of the intrinsic EC fluctuation is more complex than a concentration peak caused by a slug injection. Typically, two troughs occur within 24 hr, a deep trough in the morning and a shallow trough in the afternoon (e.g., Figure 2, p5). In addition, the flattened peaks between the troughs show small-scale fluctuations in the EC concentration. This complexity might be of advantage for distinguishing between dispersion and transient storage parameters. When dispersion was varied ($0 < D < 30$ m^2 s^{-1}) within Case 1, it affected the overall flatness of the curve, but increasing values of D completely removed small-scale fluctuations and at the same time slightly shifted all troughs to appear earlier (Figure 3). The variation of transient storage area ($0 < A_S < 5$ m^2) also led to a flattening of the overall curve. The deep troughs were dampened with increasing transient storage area, but the timing of the troughs was not affected. Interestingly, by differing in their effect on small-scale versus large-scale fluctuations, an increase in transient storage area shifts the small trough (roughly hour 95) to lower concentrations, whereas an increase in dispersion would shift it to higher concentrations, diminishing the depth of the trough. Similar to dispersion, the variation in storage rate ($-6 < \log10\ \alpha < -4$ s^{-1}) affected the small scale fluctuations more than flattening the overall curve. However, in contrast to both dispersion and transient storage area, it shifted the troughs slightly to appear later at increasing values, and it considerably changed the slope of the part of the steepest rise in EC concentration (roughly hours 85–90), while the slope of the steepest drop in concentration (roughly hours 100–105) was not affected to the same extent (Figure 3).

To compare these findings to conventional slug injections, we implemented the model using the same parameter ranges and settings on an artificial boundary concentration curve of Gaussian shape. All parameters affect the shape of the breakthrough curve as described previously (Schmadel et al., 2016) by changing the advective time (time between peaks of input and output curve), the window of detection (time between first and last detection of the output curve) and the transient storage index (time between peak and end of the output curve). Similar to the effect on the troughs in the analysis of the EC fluctuation, increasing D slightly shifted the peak of the Gaussian curve forward in time, while increasing α caused a slight backwards shift and the storage zone area did not affect the timing of the peak. Although the timing of the peak value is affected, the mean value (or expected value, which is the first temporal moment) for this model representation is not affected by D or α. The variance (second moment) is on the other hand affected by A_S, D, and α. But the variance is sometimes harder to evaluate visually due to long tails that affect moments of higher order. Analytically, increasing values of D and A_S would increase the variance, while an increase in α would decrease the variance (Riml & Wörman, 2011; Schmid, 2003).

3.3. Time Series Analysis: Solute Transport Variation Over Time

Consecutive analysis of the EC time series on the reach (Stations A–C) resulted in 2016 48-hr windows that converged, of which 1986 (88% of all windows) reached a Courant-Friedrichs-Lewy condition <1 (Figure 5). Generally, the results of all four estimated parameters showed low scattering and narrow confidence intervals in the first half of the study period, suggesting high confidence in the results. In contrast, in the second half of the study period, roughly starting with the first major rain event (hour 1,200), higher scattering of parameter estimates and time patches of wide confidence intervals were observed. A_S and D did not show a significant trend over time (Mann-Kendall test, p-value > 0.05) and varied around the median values (D: 1.1 m^2 s^{-1}; A_S: 1.1 m^2). For α a slight significant drop in values was observed from 3.1 * 10^{-5} s^{-1} (median of first 7 days) to

19447973, 2023, 7, Downloaded from https://agupubs.onlinelibrary.wiley.com/doi/10.1029/2022WR034203 by Paul Scherrer Institut PSI, Wiley Online Library on [20/07/2023]. See the Terms and Conditions (https://onlinelibrary.wiley.com/terms-and-conditions) on Wiley Online Library for rules of use; OA articles are governed by the applicable Creative Commons License

$1.3 * 10^{-5}$ s^{-1} (median of last 7 days) with an overall median of $2.0 * 10^{-5}$ s^{-1} ($z = -5.8$; p-value < 0.05). A continuously increased over time from 2.3 m^2 (median of first 7 days) to 3.7 m^2 (median of last 7 days) with an overall median of 2.7 m^2 ($z = 9.1$; p-value < 0.05). The 60% increase in A was mostly related to an increase in t_{adv} (Figure S11 in Supporting Information S1) and thus a reduction in stream velocity since Q_{av} showed no major increasing trend over time, although it was roughly 10% higher in the last 7 days (0.54 m^{-3} s^{-1}) compared to the first 7 days (0.50 m^{-3} s^{-1}) of the study period (Figure 5). Moving average air temperature (Figure 5), as well as water temperature (Figure S2 in Supporting Information S1), were rising during the study period. The average of mean water temperature of all 48-hr windows was 16.9°C and varied within 48 hr on average from +8% (90th percentile) to −9% (10th percentile).

One apparent major gap of converged windows appeared roughly at hour 900 when boundary data appeared blurry likely due to logger malfunction. Windows of high RMSE (poor fit) were found during the times of the two major rain events at hours 1,280 and 1,666. Coincidentally, the largest rain event (hour 1,666) took place at the time of mowing the macrophytes from Section 1. The steep drop in EC right after was not related to the mowing, but to the fact that the WWTP received high loads of rain water, which diluted the wastewater and therefore the discharge into river Erpe showed particularly low EC after the rain event. Both, the high discharge and the disturbance of the EC-fluctuations might have caused the high RMSE.

Zooming in on a 2-week period during a time of low variation and narrow confidence intervals (hour 500–836), slight 24-hr patterns in the time series of parameter values were found (Figure S9 in Supporting Information S1). Small-scale low points in A_S, D, and α concur with the troughs in EC at Station A which appear regularly at 7:30 a.m. each day. The highest RMSE coincides with the single hour of rainfall in the 2-weeks time frame.

Starting at hour 1,287, time series analysis was also applied separately to Section 1 (Stations A–B) and Section 2 (Stations B–C) in order to assess possible differences in parameter estimations between the sections and to assess possible change in parameters before and after mowing of Section 1. The results are given in Figure S10 in Supporting Information S1. Analysis of Section 1 resulted in 869 windows (89%) with valid solutions, while in Section 2 643 windows (66%) obtained valid solutions. In the same time period, analysis of the reach resulted in 803 (83%) windows with valid solutions. Sections 1 and 2 differed particularly in the transient storage parameters A_S and α with considerably higher overall values in Section 1 (Figure S10 in Supporting Information S1). However, as seen in the change in A for instance, mowing appears to have had a major impact on solute transport in Section 1. To illustrate the effect of mowing, the distribution of results comparing 377 hr before (bm) and 377 hr after mowing of Section 1 (am) is shown in Figure 6.

Median values of the model parameters A_S, A, and α were higher in Section 1 than Section 2, while median D was higher in Section 2 than Section 1. t_{adv} was generally lower in Section 1, because it was shorter than Section 2, but median velocity u was also lower (Figure S12 in Supporting Information S1). F_{med} in Section 1 was generally higher. The median DaI was lowest in Section 1 after mowing and Section 2 before mowing. The analyses of Section 1 resulted in lower RMSE compared to Section 2 and reach analyses. The mowing did not cause higher difference in A_S and α than the difference between sections. However, D was increased and A was decreased after mowing in Section 1. t_{adv} was clearly decreased by mowing and also DaI was considerably lower after mowing in Section 1. For the whole reach analyses (except for t_{adv} and DaI), median values were between Sections 1 and 2 median values and similar bm and am. Due to the wide distribution of results in parameter estimates of A_S and α Section 2 bm, derived metrics like T_{sto} and F_{med} showed wide distributions there compared to Sections 1 and 2 am, corresponding with high RMSE at the same time. The median storage zone residence time was higher after mowing than before mowing in Section 1 (Figure S12 in Supporting Information S1).

3.4. Tracer Injection Analysis

All approaches to estimate transport parameters of the two slug tracer injections using OTIS-P resulted in non-convergences. Therefore, a Monte Carlo sensitivity was conducted as described for the example cases of the EC curves. The scatter plots show that the RMSE is not converging toward a clear minimum for the transport parameters A_S and α, which indicates lack of sensitivity, that is, the parameters did not influence the model output (Figures S6 and S7 in Supporting Information S1). This means the recorded tracer curves are insensitive to the OTIS model parameters. A reason could be the truncation of the breakthrough curves below 0.1 µg L^{-1}, which was the detection limit of the fluorometers. Especially for the curves at Station B, this led to a low representation

19447973, 2023, 7, Downloaded from https://agupubs.onlinelibrary.wiley.com/doi/10.1029/2022WR034203 by Paul Scherrer Institut PSI, Wiley Online Library on [20/07/2023]. See the Terms and Conditions (https://onlinelibrary.wiley.com/terms-and-conditions) on Wiley Online Library for rules of use; OA articles are governed by the applicable Creative Commons License

of the tailing in the analyzed data (Romeijn et al., 2021). To test whether model parameter estimates based on the 48-hr EC curves are suitable to model theoretical concentration curves, the parameters of all 48-hr windows that contain the 8-hr recording of the tracer tests were used to model theoretical concentration curves at Station B (Figure 6). The measured tracer concentration at Station A was used as boundary condition and each set of estimated OTIS-P parameters was used to calculate a concentration curve using OTIS. It has to be noted that the results of the modeled curves using the estimated parameters cannot be directly compared to the measured breakthrough curve at station B due to the different time-scale of the tracer injection (roughly 8 vs. 48-hr windows). Average discharge within the 48-hr windows (Injection 1: ranging from 0.52 $m^3\ s^{-1}$ to 0.85 $m^3\ s^{-1}$; Injection 2: 0.47–0.49 $m^3\ s^{-1}$) varied and differed to the average discharge during tracer injections (Injection 1: 0.58 $m^3\ s^{-1}$; Injection 2: 0.57 $m^3\ s^{-1}$). The variation in discharge within the 8 hr of the 48-hr windows covering injection 1 results from the start of the major rain event causing a steep rise in discharge. The average discharge among the 48-hr windows surrounding Injection 2 was relatively constant, but lower compared to the average discharge during the 8 hr of injection, because the 8 hr were recorded in daytime, where discharge is generally higher than at night. To make the modeled tracer curves better comparable to the recorded tracer curves, the modeled parameters of the 48-hr windows were used, but the discharge was set to the average discharge during injection (Figure 7). A version of the comparison, where the original varying average discharge values were used is shown in Figure S13 in Supporting Information S1. The equal-discharge comparison shows that the height and the timing partly coincide (Figure 7). Few of the modeled curves using the estimated parameters of 48-hr windows surrounding Injection 1 resemble the shape of the measured tracer curve. This can be attributed to the steep rise in average discharge and with it cross-section area A (3.3–9.6 m^2). As the discharge was set to 0.58 for all curves, the variation in A affected the first temporal moment of the curves shifting it backwards in time. In contrast, the curves derived from different 48 hr-windows surrounding Injection 2 were found to be relatively similar to each other, and resembled the shape of the measured breakthrough curve due to more stable discharge conditions and therefore less variation in A in that period (2.93–3.22 m^2). However, they occurred slightly earlier compared to the measured tracer curve. An explanation could be that discharge and therefore the cross section area A during the 8 hr of injection was on average higher compared to the 48-hr window analyses which shifted the first temporal moment to occur slightly later.

4. Discussion

4.1. Sensitivity of Parameter Estimations in Example Cases

The scatter plots of the Monte-Carlo sensitivity analysis (Figure 2) show that none of the selected cases result in equifinality of model parameters, as the RMSE displays minimum values corresponding to well-defined parameter sets. In Suite 3, where parameter ranges are narrowed down in vicinity of the global minimum of RMSE, all cases "dip" toward a particular parameter combination, displaying a high degree of sensitivity in the RMSE to changes in parameter values (as termed by Ward et al., 2017). Equifinality would appear merely on considerably small parameter scales in the tested cases, so uncertainties in the estimated parameters are interpreted as low. Also the visual comparison between modeled and measured concentration curves at Station C (Figure 2: p5, p10, p15), confirm appropriate performance of OTIS to reproduce the solute transport behavior. Among the different cases, the model appeared most sensitive to the parameters in Case 2 with scatter plots showing the most pronounced minima (Figure 2). In this case the steep troughs in the EC curves window possibly helped to better constraint the model parameters. The analysis did not only show that the model was sensitive, it also confirmed that OTIS-P managed to locate the global minima and did not merely converge to a local minimum as a consequence of the initial values of the model parameters. Although the Monte-Carlo analysis found solutions of lower RMSE than OTIS-P, the results were comparable and in the majority of the comparisons the best fits of the sensitivity analysis were within the 95% confidence interval given by OTIS-P. Hence, the Monte-Carlo sensitivity analysis in general gave rise to confidence in the OTIS-P results to converge at global minima and to achieve reasonable best fits; moreover, it confirmed that the model output was sensitive to the transport processes tracked by EC fluctuations.

The Sobol analysis generally confirmed the findings of the Monte-Carlo analysis. All parameters influenced the RMSE throughout the different tests (Figure 3). However, if the threshold of 0.25 for first-order indices is applied, as used by Kelleher et al. (2013), D is not considered sensitive in any tested parameter range-case combination (Table S2 in Supporting Information S1). For A, A_S and α, in contrast, whenever the total-order index was calculated to be >0.25, the first order index was >0.25 as well, and the share of the first order within the total order

19447973, 2023, 7, Downloaded from https://agupubs.onlinelibrary.wiley.com/doi/10.1029/2022WR034203 by Paul Scherrer Institut PSI, Wiley Online Library on [20/07/2023]. See the Terms and Conditions (https://onlinelibrary.wiley.com/terms-and-conditions) on Wiley Online Library for rules of use; OA articles are governed by the applicable Creative Commons License

index was at least 69%, meaning in this case less than 31% of output variance was caused by parameter interactions (except for A, and α in Case 2 within the time-series boundaries). The generally large first order indices point to the small interaction between parameters. The relative high independence between parameters contrasts previous findings of studies using slug injections, were OTIS-P parameters were found to be highly interactive (Gooseff et al., 2005; Kelleher et al., 2013). However, A, A_S and α were not sensitive in all parameter range-case combinations. For example, in Case 3 within the 5th and 95th percentiles of parameters estimated in the time series analysis, A was not sensitive. But between Cases 1–3, all three parameters were sensitive at least once. For the time series analysis, this means that within the distribution of 48 hr-window analyses some of them might result in high uncertainty for single parameters. This disadvantage is outbalanced with the high amount of 48-hr windows considered, as single results with high uncertainty might appear as noise within the time series.

4.2. Breakthrough Curve Analysis

The sensitivity analysis strengthened the conjecture that EC fluctuations can be used to estimate solute transport metrics. However, the question remained: why is it in the current analysis possible to distinguish the transient storage parameters, although the EC curves did not contain a tail of a traditional slug injection? In fact, Drummond et al. (2012) found in a study on 167 tracer injections, that tail truncation of the breakthrough curve can lead to an underestimation of solute exchange and solute retention. This has also been demonstrated in other studies suggesting that in tracer induced breakthrough curves a lot of information on the transient storage parameters lays in the tail (e.g., Harvey & Wagner, 2000; Wörman & Wachniew, 2007) and that a missing tail can lead to high uncertainty in such experiments.

In the breakthrough curve analysis we showed that D, A_S and α affect the EC curve in different ways compared to a classic breakthrough curve (Figure 4). In contrast to a conventional slug-injection curve the more complex EC signal comprised small-scale fluctuations including a second shallow trough roughly 12 hr after the major trough. For example, while all parameters shift the major trough to lower concentrations at higher values, the shallow trough is dampened by increasing D and α, but it is raised with increasing A_S. The findings suggest that complex continuous signals of environmental tracers such as EC, can effectively constrain model parameters similar to conventional slug injections. The complexity of the curve can therefore overcome the disadvantage of a missing tail in conventional slug injections. This phenomenon is related to the concept of a signal's entropy in information theory, which is the amount of information it may convey (Shannon, 1948). In the Sobol analysis we showed that the signal contains information on all the tested parameters to some extent, as variation of all parameters influenced the modeled signal and thus the RMSE. Only D showed little identifiability in the Sobol analysis, as well as the breakthrough curve analysis, where variation in D on a scale of 0–30 $m^2\ s^{-1}$ only affected the curve marginally compared to the effects of A_S and α. To the best of our knowledge, the only other study that used the transient storage model on environmental solute concentration data was conducted by Ryan et al. (2004). There, the missing tail is addressed in the discussion by stating that the "conclusions are somewhat obscured" by the lack of long tailing.

A quantitative comparison of identifiability of parameters between traditional injected tracers and intrinsic fluctuating curves is outside the scope of this study. However, even if the intrinsic tracers perform worse in identifying certain parameters at a time, the advantage of having a large amount of breakthrough curves available will outweigh the disadvantage of a potentially weak model performance during specific time periods.

4.3. Impact of Discharge Fluctuation

A major difficulty of using intrinsic EC fluctuation for modeling solute transport with the transient storage concept is how to handle unsteady flow conditions. In fact, EC dynamics in the effluent of a WWTP are generally associated with discharge fluctuations. Discharge can considerably impact transient storage and the solute transport model performance as well as bulk solute transport via changes in velocity and dispersion (Schmadel et al., 2016; Ward et al., 2019). The OTIS model has a function to implement unsteady boundary conditions, that is, changing discharge, but in addition to the time-varying discharge it requires the co-occurring change in A as input. Due to the lack of observations over time, estimation of varying A would be highly uncertain and would render the results of the unsteady model rather speculative. Also, while the unsteady OTIS model implements changing discharge, the parameter estimates remain lumped in time and space, that is, a parameter averaged over

10.1029/2022WR034203

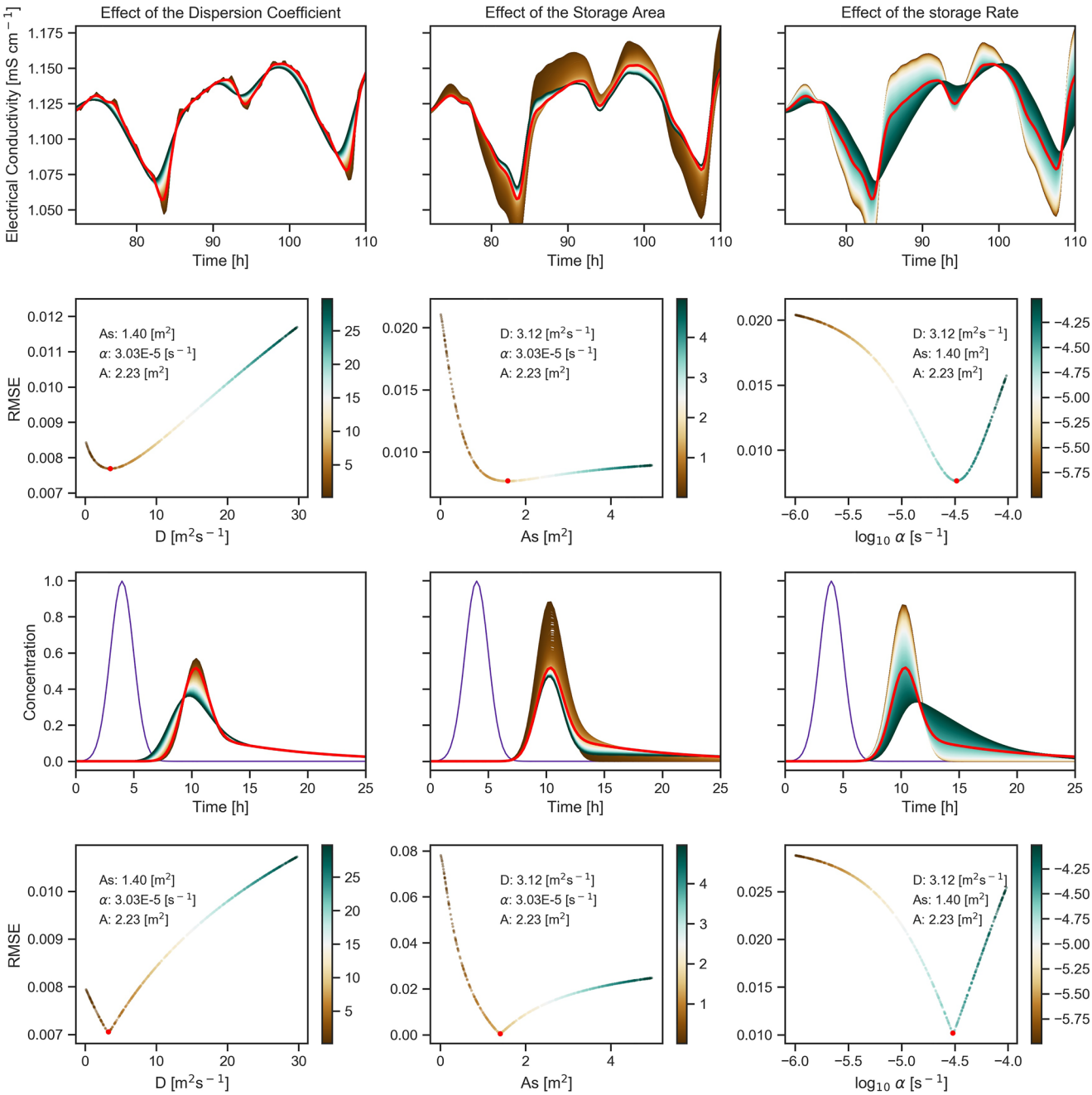

Figure 4. Row 1: Effects of variations of dispersion coefficient (D), storage area (As) and storage rate (α) on the calculated electrical conductivity (EC) time series at Station C using the 48-hr EC time series of Station A recorded in April as input (Case 1). The color scale indicates the variations of the respective parameter. Row 3: Simulation of effects of variations of dispersion coefficient (D), the storage area (As) and the storage rate (α), respectively, on the break through curve of a theoretical artificial slug injection under the conditions of Case 1. First peaks (purple) show the input time series at Station A (not shown in the Row 1 for better visibility) while the second peaks are the calculated time series at Station C for variations of dispersion coefficient, storage area and storage rate. The plots in Rows 2 and 4 show the changes in Root mean squared error (RMSE) with the variation of the respective parameters. The red points indicate the smallest RMSE and red lines indicate the curve of best fit. Note: Plots within the dashed boxes belong to the same analysis. Color scales of the variations in breakthrough curves are given in the color bars of the plots below.

time is provided. The steady model using the average discharge still reproduces the EC breakthrough curves relatively well returning low RMSEs and converging to the best fit in most cases. The major discrepancies between modeled and measured curves occur in a double-peak of residuals during the steep slope, which correspond to fast decreases of EC toward major troughs. The correlation of discharge and residuals in Cases 1 and 2 indicate

19447973, 2023, 7, Downloaded from https://agupubs.onlinelibrary.wiley.com/doi/10.1029/2022WR034203 by Paul Scherrer Institut PSI, Wiley Online Library on [20/07/2023]. See the Terms and Conditions (https://onlinelibrary.wiley.com/terms-and-conditions) on Wiley Online Library for rules of use; OA articles are governed by the applicable Creative Commons License

10.1029/2022WR034203

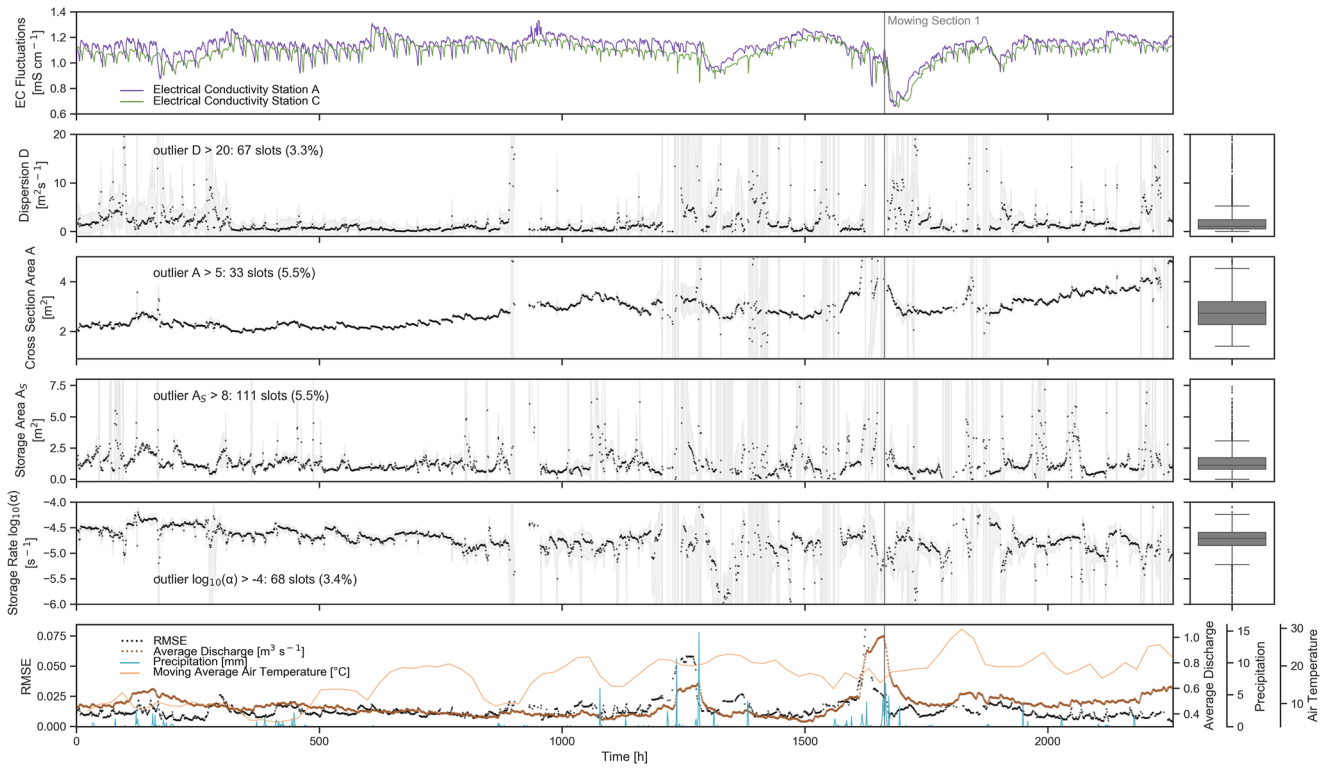

Figure 5. Time series analysis of 48-hr windows of electrical conductivity (EC) fluctuations in hourly steps using OTIS-P. Row 1: Time series of EC at stations A and C. The parameters resulting from the converged windows are shown as black dots in Rows 2–5, respectively, for the start time of each window (TSTART) in black dots. Transparent gray areas indicate the confidence interval (95%) calculated by OTIS-P. The number of outliers (and respective percentage of all converged windows) that are not shown for clarity are given in Rows 2–5 where applicable. The boxplots show the distribution of parameters in that row over the whole study period. In Row 6 the root mean squared error of each window, the average discharge of each window, the average daily temperature and the precipitation are shown.

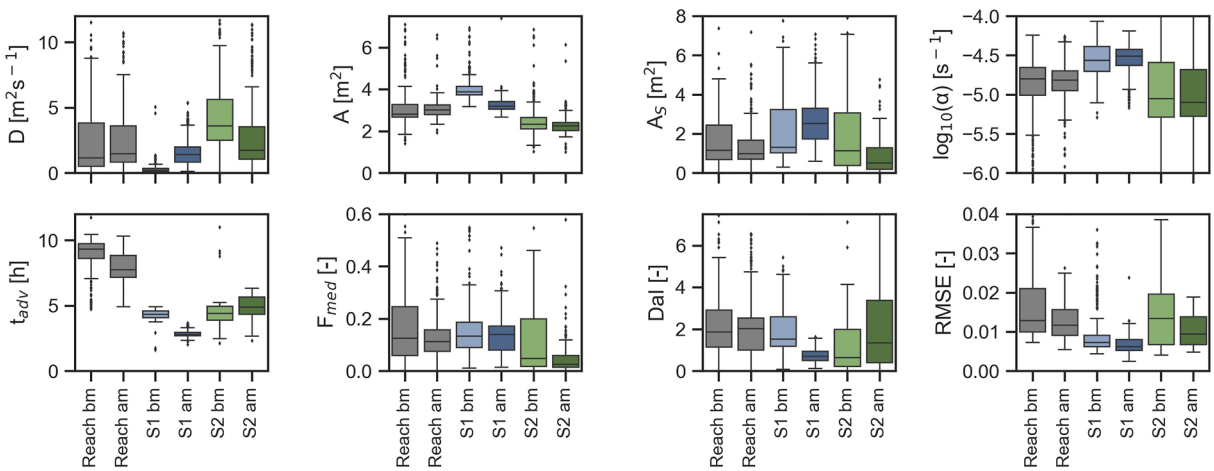

Figure 6. Distribution of estimated parameter values and metrics (dispersion coefficient [D], cross sectional area [A] storage area [A_S], storage rate [α], advective travel time [t_{adv}], F_{med}, Damköhler number [DaI] and root mean squared error [RMSE]) within 377 hr for Section 1 before (S1bm; $n = 298$) and after (S1am; $n = 370$) mowing and Section 2 before (S2bm; $n = 263$) and after (S2am; $n = 295$) mowing, respectively. For comparison the distributions of parameters in the same time frames of the whole reach analysis are given before (Reach bm; $n = 290$) and after (Reach am; $n = 324$) mowing. Outliers, as well as parts of the whiskers of $\log_{10}\alpha$, were partly cut off in the graphs for better visibility.

19447973, 2023, 7, Downloaded from https://agupubs.onlinelibrary.wiley.com/doi/10.1029/2022WR034203 by Paul Scherrer Institut PSI, Wiley Online Library on [20/07/2023]. See the Terms and Conditions (https://onlinelibrary.wiley.com/terms-and-conditions) on Wiley Online Library for rules of use; OA articles are governed by the applicable Creative Commons License

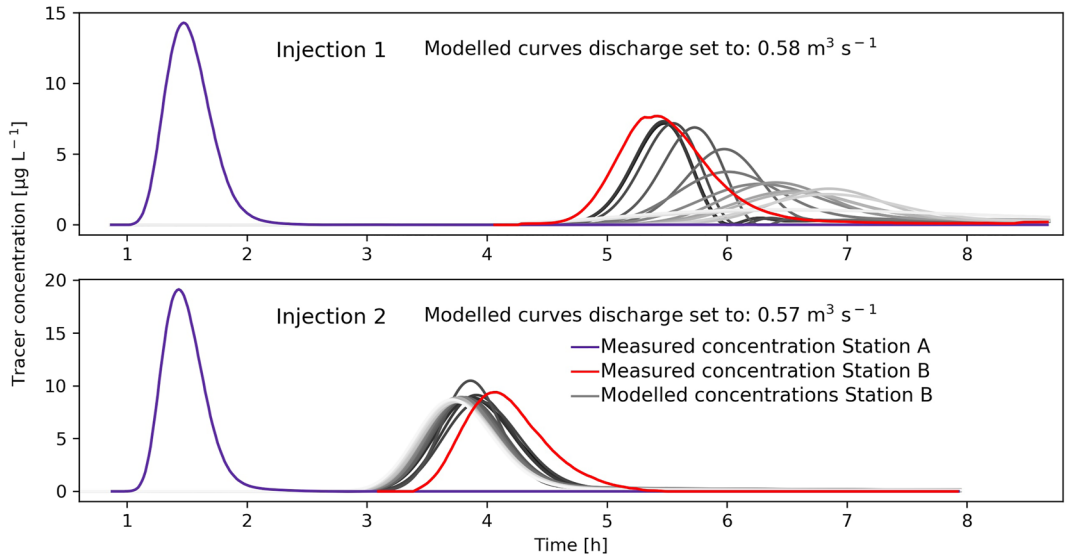

Figure 7. Measured breakthrough curves of fluorescein at Station A (purple) and Station B (red). For comparison the concentration curves modeled with one-dimensional transport with inflow and storage using the estimated parameters of all the 48-hr windows that contain the 8 hr of tracer recording and returned valid solutions in the time series analysis are plotted in gray-scale (Injection 1: $n = 16$; Injection 2: $n = 24$). The gray-scale indicates the temporal order of the 48-hr windows from dark indicating the first to bright indicating the last.

that the discharge fluctuations that are not accounted for in the model are responsible for the misfit (Figure S8 in Supporting Information S1).

4.4. Performance of the Model Using a Time Series of EC

The uncertainties of the time series model parameter estimates indicated by the width of the confidence intervals were considerably lower in the first part of the study period. A possible explanation is the low amount of rain events and the lower presence of macrophytes in the first part of the time period (Figure 4). Hence, in this period from early April to mid of June, the flow was rather undisturbed and the discharge relatively regular. In the second part of the time series, quick rises in Q_{av} caused by increased discharge from the WWTP at heavy rain events and increased presence of macrophytes could be responsible for the wider confidence intervals compared to the first part. The relation of model performance to precipitation and rise in Q_{av} is also reflected in rising RMSE (Figure 4). The reason, that confidence intervals partly remain wide after the second high rain event from roughly hour 1,700 despite little precipitation and low change in Q_{av} might be the regrowth of macrophytes after mowing of Section 1 and generally higher abundance of macrophytes in Section 2 compared to the beginning of the study period (Kurz et al., 2017). 48-hour windows that did not converge occur in clusters close to rain events, where the regular EC fluctuations were disturbed. In addition, between hour 900 and 1,000 logger malfunction at Station A seemed to have caused a cluster of consecutive non-convergences. The vague 24-hr pattern observed in the parameter time series (Figure S9 in Supporting Information S1) indicates that the model results were slightly affected by the position of TSTART within the daily fluctuation, but did not obscure the overall time trend. In conclusion, the method of time series analysis presented here performed best in times of low precipitation and low macrophyte abundance.

Despite the noisiness of estimated parameters in the time-series and partly wide confidence intervals, the majority of 48-hr windows provide reasonable estimates, especially in the first part of the study time. The comparison of the independent experiment of two tracer injections during the study time supports the general results. The modeled curves using the parameter estimates of the 48 hr-windows reasonably resemble the measured curves of the tracer injections, especially considering the distinct difference between injection 1 and 2 caused by the mowing of Section 1 and the different methods of recording (fluorescein injection vs. internal EC fluctuation), as well as the differences in time-scales (tracer injection of 8 vs. the 48-hr windows). This confirms that the OTIS-P estimates yield reasonable parameters that represent the different

19447973, 2023, 7, Downloaded from https://agupubs.onlinelibrary.wiley.com/doi/10.1029/2022WR034203 by Paul Scherrer Institut PSI, Wiley Online Library on [20/07/2023]. See the Terms and Conditions (https://onlinelibrary.wiley.com/terms-and-conditions) on Wiley Online Library for rules of use; OA articles are governed by the applicable Creative Commons License

19447973, 2023, 7, Downloaded from https://agupubs.onlinelibrary.wiley.com/doi/10.1029/2022WR034203 by Paul Scherrer Institut PSI, Wiley Online Library on [20/07/2023]. See the Terms and Conditions (https://onlinelibrary.wiley.com/terms-and-conditions) on Wiley Online Library for rules of use; OA articles are governed by the applicable Creative Commons License

solute transport conditions of the river at different time points. The wide spreading of the model results in injection 1 resulted from the high differences in average discharge and the cross section area among the 48-hr windows, which coincided with the time of a major rainfall event (Figure 7 and Figure S13 in Supporting Information S1).

4.5. Interpretation of Time Varying Model Parameters

While the study focuses on presenting a novel method to continuously record solute transport behavior across seasons, the practical example of river Erpe revealed some interesting trends in transport parameters. In contrast to our hypothesis that macrophyte growth between April and July will continuously increase the transient storage zone A_S across the seasons, the parameter displayed no increasing trend during the study period on the reach-analysis (Figure 5, Mann-Kendall test not significant). Instead, the cross section Area A was significantly increasing within the time of the study. In the same time, discharge Q_{av} did not show a rising trend leading to a gradual increase in the advective travel time t_{adv} (Figure S11 in Supporting Information S1). Probably, the growth of macrophytes influenced the solute transport by retarding the flow in the main channel, increasing t_{adv} and A to a higher degree than the transient storage parameters, when evaluated for the whole reach. Likely, the macrophytes covered the channel to an extent that there was no main channel flow unaffected by the plants, which is not unlikely for submerged vegetation (Kubrak et al., 2008). Also, the channelized character of the river might have hindered the spreading of the water to side pockets, which would have increased the storage area as opposed to the main channel area. In a more natural alluvial stream, growth of macrophytes led to a widening of the channel and subsequent increase in A_S/A ratio (Harvey et al., 2003). A widening of the channel in river Erpe is not possible due to the steap and partly reinforced river banks. Hence, the macrophytes did apparently not create additional pockets of retarded streamflow, but instead reduced the bulk flow velocity of the main channel. Rising water temperature (Figure S2 in Supporting Information S1) potentially also affects water transport properties. With increasing temperature the viscosity decreases and can lead to higher hyporheic exchange (Wu et al., 2020). However, rising water temperature apparently did not affect the exchange rates, as α decreased over time. The slight significant drop in α could be caused by macrophytes on the sediment surface hindering quick exchange with the shallow hyporheic zone to some extent.

Also F_{med} and DaI did not show a consistent trend over time on the whole reach analysis, but their variability increased in the second half of the study time, likely related to higher precipitation and presence of macrophytes (Figure S11 in Supporting Information S1).

Median DaI were generally close to 1 (0.6–1.5) in all section analyses, while reach scale analyses were close to 2. Therefore advection to transient storage interaction timescale ratio was more ideal for transient storage analysis in the sections, as DaI close to 1 indicates a balance between advection and transient storage parameters. Wagner and Harvey (1997) analyzed designs of tracer studies and found, that the reliability of resulting transport parameters considerably depended on the DaI. They stated that DaI values much smaller or higher than 1 lead to high parameter uncertainties. In these cases either the stream velocity is too high in relation to the exchange timescale so too little solute is interacting with the storage zone or the solute exchange happens so fast compared to the stream velocity, so that all solute is exchanged within the experimental section of the stream. For the reach scale analyses with median DaI > 1, the advection timescale overweights the interaction timescale due to the longer stream section slightly, however reliability of transient storage parameters was not impeded as the timescales were within the order of 1.

Mowing in Section 1 affected both timescales. Overall, the DaI was reduced by mowing, hence the advection to interaction timescale ratio decreased. The advection timescale got reduced as t_{adv} and A decreased. The interaction timescale increased by increasing A_S. Interaction rate α increased as well after mowing, potentially caused by increase in small-scale hyporheic exchange after the removal of macrophytes, but it did not outweigh the effect of increase in storage zone and, thus, overall reduction of the DaI caused by the other parameters.

In contrast, in Section 2 the median DaI was lower before mowing. As t_{adv} and A were relatively close in Section 2 before and after mowing the change might have been caused by higher A_S before mowing. However, the distributions of estimated parameters, especially α, in Section 2 after mowing is relatively wide. Also, the RMSEs in Section 2 were higher than in Section 1, indicating higher uncertainty of the values, which renders the comparison of DaI median values more unreliable than in Section 1.

19447973, 2023, 7, Downloaded from https://agupubs.onlinelibrary.wiley.com/doi/10.1029/2022WR034203 by Paul Scherrer Institut PSI, Wiley Online Library on [20/07/2023]. See the Terms and Conditions (https://onlinelibrary.wiley.com/terms-and-conditions) on Wiley Online Library for rules of use; OA articles are governed by the applicable Creative Commons License

Median F_{med} representing the median travel time that is caused by transient storage, remained below 0.2 in all sections before and after mowing. Therefore, the portion of median travel time due to storage was below 20% of the total reach travel time, however more than 10% in the reach analysis and in Section 1. The metric is mainly controlled by A_S which shows the same trend among the six situations (Reach bm, Reach am, Section 1 bm, Section 1 am, Section 2 bm and Section 2 am) as F_{med}. Median F_{med} is generally higher in Section 1 compared to Section 2. In Section 1 after mowing F_{med} is highest, so transient storage contributes most to the median travel time. As F_{med} is inversely related to travel time (see Equation 6), the reduction in t_{adv} caused by the mowing, in combination to the increased A_S were responsible for to the slightly higher median F_{med} in Section 1 after mowing. Median T_{sto} also increased after mowing in Section 1, because A_S increased and A decreased. The high distribution of T_{sto} in Section 2, particularly before mowing is attributed to high uncertainty in the estimates parameters, and potentially high outliers in α in this Section.

DaI, T_{sto} and F_{med} show that mowing in Section 1 led to a slight relative increase in transient storage. Irrespective of the reduction in t_{adv}, higher median A_S occurring after mowing indicates also an absolute increase in transient storage. This observation agrees with the independent analysis of the tracer injections in river Erpe originally described by Romeijn et al. (2021). Comparing several slug tracer injection before and after mowing along Section 1, transient storage indices were found to have increased. A study in Säva Brook, an agricultural stream in Sweden, found that transient storage metrics were higher in vegetated streams compared to unvegetated. There, mowing led to a decrease in the exchange rate (Salehin et al., 2003). Also other studies found a positive impact of vegetation on hyporheic exchange (Huang & Yang, 2022; Kurz et al., 2017). Harvey et al. (2003) found an increased ratio of A_S/A over a study time of 5 years in a stream with increasing presence of macrophytes in a desert stream, which at the same time increased the channel width. Reasons for the contrasting results found at the River Erpe could be the morphology and composition of the streambeds and the extent and type of vegetation. Due to the channelized shape of the river, the growing macrophytes cause a vertical rise in water level, rather than a expansion of river width to a flood plain with potential formation of new storage areas. Also the method used for mowing likely affected streambed properties. The mowing could have disturbed the sediment surface in a way to reduce clogging and compaction and therefore increase shallow hyporheic exchange (Nogaro et al., 2010). Also higher flow velocity after mowing might have had a beneficial impact on the hyporheic exchange (Boano et al., 2014) In addition, the type of vegetation has a high influence on the velocity distribution, depending also on stem density and flexibility. Emerged vegetation, as present in River Erpe, covering the whole cross section can cause more uniform velocity distributions as opposed to submerged vegetation (Kubrak et al., 2008).

Although median F_{med} are clearly higher in Section 1 compared to Section 2, likely controlled by higher A_S, median DaI are not lower in Section 1. Here the high median α values might have outweighed the higher median A_S. An interpretation could be that the characteristics of Section 1 favor quick shallow hyporheic exchange over long-term hyporheic flow paths.

In a previous study investigating the fate of micropollutants in the same reach, the biodegradable compounds metoprolol and valsartan showed generally higher degradation in Section 1 compared to Section 2. Additionally, the transformation products metoprolol acid and valsartan acid showed higher formation in Section 1 compared to Section 2 even after removal of macrophytes. The authors suspected that the difference in transformation capacity between the two sections derives from the difference in transient storage (Jaeger et al., 2019). This assumption can be confirmed with the results of the present study. Some of the compounds (bezafibrate, metformin and guanylurea) showed higher attenuation after mowing compared to before mowing in Section 1 and photolysis was excluded as a reason. Higher transient storage in the form of increased shallow hyporheic exchange after mowing was described as a possible factor. This theory is more likely after considering the findings of the present study. The combination of the results of both studies strengthens the idea that transient storage promotes the removal capacity of certain micropollutants in lowland rivers.

5. Conclusion

The approach to estimate time series of solute transport metrics from daily intrinsic fluctuation of EC proved to be a feasible low-cost option that can provide useful insights in spatially and temporally varying flow conditions.

Although the fluctuation in discharge in combination with the steady-state assumption of the transport model is not ideal for the model fits and continuous EC records do not include the long tails of tracer breakthrough

19447973, 2023, 7, Downloaded from https://agupubs.onlinelibrary.wiley.com/doi/10.1029/2022WR034203 by Paul Scherrer Institut PSI, Wiley Online Library on [20/07/2023]. See the Terms and Conditions (https://onlinelibrary.wiley.com/terms-and-conditions) on Wiley Online Library for rules of use; OA articles are governed by the applicable Creative Commons License

curves, which are typical of slug injections, we could show that reliable transport metrics can be extracted from the EC time series. Notably, the shapes of the breakthrough curves were sensitive to the transient storage parameters despite the missing tails. The strength of the approach discussed in the present study lays in the ease of acquiring long-term records and, hence, a large amount of data. The approach leaves room for occasional model failures (non-convergence), outliers and values of high uncertainty. But the assessment revealed that numerous consecutive model runs provided coherent information on the transient storage metrics especially at times of low precipitation and low presence of macrophytes. Even in periods where no time-trend can be observed, the dynamics of solute concentration can provide more realistic information about solute transport and retention processes in stream waters compared to analysis of time-limited snap-shots obtained from artificial tracer injections. The rejection of our preliminary hypothesis that the transient storage zone increases with increasing growth of macrophytes is an ideal example for valuable information that could only be obtained by the means of a time series of A and A_S across seasons.

There is also potentially high value in using intrinsic-tracer analysis in combination with artificial tracer injections for mutual validation or comparisons. Knapp and Kelleher (2020) point out that single tracer experiments should be ideally combined with other environmental data as their combination can contribute to develop novel research questions. In the present case, the novelty lies especially in the additional large temporal scale that can complement the information traditionally obtained from tracer experiments.

Practical application of the presented method can be of particularly high interest for river management. Preliminary information on gradual changes of solute transport dynamics across the seasons can facilitate planning of effective and sustainable restauration and management measures. In addition, it can contribute to a comprehensive post-implementation monitoring and assess the successfulness of restoration on a longer timescale. Measurements for reducing siltation and enhancing hyporheic exchange, for instance, like introducing boulders or woody debris, can be examined by their impact on solute transport (Blaen et al., 2018; Grabowski et al., 2019; Marttila et al., 2018). Other common management techniques, like the removal of macrophytes, can be tested for their side-effects on solute transport. Time series data can potentially also serve to evaluate different methods' long-term capacities to promote biochemical cycles, to benefit attenuation of nutrients and contaminants and safeguard ecosystem health in general.

To conclude, regular EC fluctuations in wastewater-impacted rivers are a very valuable feature to be made use of. Although the approach of the present study highlights the potential, it is only a first step. Ideally, future studies will consider more elaborate solute transport models, for example, accounting for different representations of the often diverse and complex transient storage processes, and also explicitly represent unsteady flow conditions. Also, analysis of longer time series, for example, comparing different years, would be of high interest for river restoration practitioners. The storage zone development of a newly restored river section could for instance be tracked. The rapid automated analysis of reoccurring fluctuations can open doors for numerous novel research questions in solute transport analysis and might eventually enable the development of continuous transient storage monitoring.

Conflict of Interest

The authors declare no conflicts of interest relevant to this study.

Acknowledgments
The work has received funding from the European Union's Horizon 2020 research and innovation programme under Marie Sklodowska-Curie grant agreement No 641939 and additionally from the Research Training Group "Urban Water Interfaces (UWI)" (GRK 2032/1) funded by the German Research Foundation (DFG). We also thank all members of the HypoTrain project and the IGB Berlin laboratory technicians for their valuable help and contributions. Open Access funding enabled and organized by Projekt DEAL.

Data Availability Statement

The data analyzed in this paper can be found at https://doi.org/10.18728/igb-fred-803.0 published as Jaeger (2022).

References

Bahr, J. M., & Rubin, J. (1987). Direct comparison of kinetic and local equilibrium formulations for solute transport affected by surface reactions. *Water Resources Research*, *23*(3), 438–452. https://doi.org/10.1029/WR023i003p00438

Bencala, K. E. (1983). Simulation of solute transport in a mountain pool-and-riffle stream with a kinetic mass transfer model for sorption. *Water Resources Research*, *19*(3), 732–738. https://doi.org/10.1029/WR019i003p00732

Bencala, K. E., & Walters, R. A. (1983). Simulation of solute transport in a mountain pool-and-riffle stream: A transient storage model. *Water Resources Research*, *19*(3), 718–724. https://doi.org/10.1029/WR019i003p00718

Blaen, P. J., Kurz, M. J., Drummond, J. D., Knapp, J. L. A., Mendoza-Lera, C., Schmadel, N. M., et al. (2018). Woody debris is related to reach-scale hotspots of lowland stream ecosystem respiration under baseflow conditions. *Ecohydrology*, *11*(5), e1952. https://doi.org/10.1002/eco.1952

Boano, F., Harvey, J. W., Marion, A., Packman, A. I., Revelli, R., Ridolfi, L., & Wörman, A. (2014). Hyporheic flow and transport processes: Mechanisms, models, and biogeochemical implications. *Reviews of Geophysics*, *52*(4), 603–679. https://doi.org/10.1002/2012RG000417

Cirpka, O. A., Fienen, M. N., Hofer, M., Hoehn, E., Tessarini, A., Kipfer, R., & Kitanidis, P. K. (2007). Analyzing bank filtration by deconvoluting time series of electric conductivity. *Groundwater*, *45*(3), 318–328. https://doi.org/10.1111/j.1745-6584.2006.00293.x

Courant, R., Friedrichs, K., & Lewy, H. (1928). Über die partiellen Differenzengleichungen der mathematischen Physik. *Mathematische Annalen*, *100*(1), 32–74. https://doi.org/10.1007/BF01448839

Dennis, J. E., Jr., Gay, D. M., & Welsch, R. E. (1981). Algorithm 573: NL2SOL—An adaptive nonlinear least-squares algorithm (E4). *ACM Transactions on Mathematical Software (TOMS)*, *7*(3), 369–383. https://doi.org/10.1145/355958.355966

Donaldson, J. R., & Tryon, P. V. (1987). *User's guide to STARPAC, the standards time series and regression package*. Scientific Computing Division, National Center for Atmospheric Research.

Drummond, J. D., Covino, T. P., Aubeneau, A. F., Leong, D., Patil, S., Schumer, R., & Packman, A. I. (2012). Effects of solute breakthrough curve tail truncation on residence time estimates: A synthesis of solute tracer injection studies. *Journal of Geophysical Research*, *117*(G3), G00N08. https://doi.org/10.1029/2012JG002019

Glaser, C., Zarfl, C., Werneburg, M., Böckmann, M., Zwiener, C., & Schwientek, M. (2020). Temporal and spatial variable in-stream attenuation of selected pharmaceuticals. *Science of the Total Environment*, *741*, 139514. https://doi.org/10.1016/j.scitotenv.2020.139514

Gooseff, M. N., Bencala, K. E., Scott, D. T., Runkel, R. L., & McKnight, D. M. (2005). Sensitivity analysis of conservative and reactive stream transient storage models applied to field data from multiple-reach experiments. *Advances in Water Resources*, *28*(5), 479–492. https://doi.org/10.1016/j.advwatres.2004.11.012

Grabowski, R. C., Gurnell, A. M., Burgess-Gamble, L., England, J., Holland, D., Klaar, M. J., et al. (2019). The current state of the use of large wood in river restoration and management. *Water and Environment Journal*, *33*(3), 366–377. https://doi.org/10.1111/wej.12465

Haggerty, R., Wondzell, S. M., & Johnson, M. A. (2002). Power-law residence time distribution in the hyporheic zone of a 2nd-order mountain stream. *Geophysical Research Letters*, *29*(13), 18-11–18-14. https://doi.org/10.1029/2002GL014743

Harvey, J. W., Conklin, M. H., & Koelsch, R. S. (2003). Predicting changes in hydrologic retention in an evolving semi-arid alluvial stream. *Advances in Water Resources*, *26*(9), 939–950. https://doi.org/10.1016/S0309-1708(03)00085-X

Harvey, J. W., & Wagner, B. J. (2000). 1 - Quantifying hydrologic interactions between streams and their subsurface hyporheic zones. In J. B. Jones & P. J. Mulholland (Eds.), *Streams and ground waters* (pp. 3–44). Academic Press.

Huang, S., & Yang, J. Q. (2022). Impacts of emergent vegetation on hyporheic exchange. *Geophysical Research Letters*, *49*(13), e2022GL099095. https://doi.org/10.1029/2022GL099095

Jaeger, A. (2022). *River Erpe electrical conductivity data summer 2016/Project HypoTrain* [Dataset]. IGB Leibniz-Institute of Freshwater Ecology and Inland Fisheries. https://doi.org/10.18728/igb-fred-803.0

Jaeger, A., Posselt, M., Betterle, A., Schaper, J., Mechelke, J., Coll, C., & Lewandowski, J. (2019). Spatial and temporal variability in attenuation of polar organic micropollutants in an urban lowland stream. *Environmental Science & Technology*, *53*(5), 2383–2395. https://doi.org/10.1021/acs.est.8b05488

Kelleher, C., Wagener, T., McGlynn, B., Ward, A. S., Gooseff, M. N., & Payn, R. A. (2013). Identifiability of transient storage model parameters along a mountain stream. *Water Resources Research*, *49*(9), 5290–5306. https://doi.org/10.1002/wrcr.20413

Kilpatrick, F. A., Wilson, J. F., & Survey, G. (1989). *Measurement of time of travel in streams by dye tracing*. U.S. Government Printing Office.

Knapp, J. L. A., & Kelleher, C. (2020). A perspective on the future of transient storage modeling: Let's stop chasing our tails. *Water Resources Research*, *56*(3), e2019WR026257. https://doi.org/10.1029/2019wr026257

Kubrak, E., Kubrak, J., & RowiŃSki, P. M. (2008). Vertical velocity distributions through and above submerged, flexible vegetation. *Hydrological Sciences Journal*, *53*(4), 905–920. https://doi.org/10.1623/hysj.53.4.905

Kurz, M. J., Drummond, J. D., Marti, E., Zarnetske, J. P., Lee-Cullin, J., Klaar, M. J., et al. (2017). Impacts of water level on metabolism and transient storage in vegetated lowland rivers: Insights from a mesocosm study. *Journal of Geophysical Research: Biogeosciences*, *122*(3), 628–644. https://doi.org/10.1002/2016jg003695

Lewandowski, J., Arnon, S., Banks, E., Batelaan, O., Betterle, A., Broecker, T., et al. (2019). Is the hyporheic zone relevant beyond the scientific community? *Water*, *11*(11), 2230. https://doi.org/10.3390/w11112230

Marion, A., Zaramella, M., & Packman, A. I. (2003). Parameter estimation of the transient storage model for stream–subsurface exchange. *Journal of Environmental Engineering*, *129*(5), 456–463. https://doi.org/10.1061/(ASCE)0733-9372(2003)129:5(456)

Marttila, H., Turunen, J., Aroviita, J., Tammela, S., Luhta, P.-L., Muotka, T., & Klöve, B. (2018). Restoration increases transient storages in boreal headwater streams. *River Research and Applications*, *34*(10), 1278–1285. https://doi.org/10.1002/rra.3364

Mechelke, J., Vermeirssen, E. L. M., & Hollender, J. (2019). Passive sampling of organic contaminants across the water-sediment interface of an urban stream. *Water Research*, *165*, 114966. https://doi.org/10.1016/j.watres.2019.114966

Nogaro, G., Datry, T., Mermillod-Blondin, F., Descloux, S., & Montuelle, B. (2010). Influence of streambed sediment clogging on microbial processes in the hyporheic zone. *Freshwater Biology*, *55*(6), 1288–1302. https://doi.org/10.1111/j.1365-2427.2009.02352.x

Nossent, J., Elsen, P., & Bauwens, W. (2011). Sobol' sensitivity analysis of a complex environmental model. *Environmental Modelling & Software*, *26*(12), 1515–1525. https://doi.org/10.1016/j.envsoft.2011.08.010

Peralta-Maraver, I., Galloway, J., Posselt, M., Arnon, S., Reiss, J., Lewandowski, J., & Robertson, A. L. (2018). Environmental filtering and community delineation in the streambed ecotone. *Scientific Reports*, *8*(1), 15871. https://doi.org/10.1038/s41598-018-34206-z

Posselt, M., Jaeger, A., Schaper, J. L., Radke, M., & Benskin, J. P. (2018). Determination of polar organic micropollutants in surface and pore water by high-resolution sampling-direct injection-ultra high performance liquid chromatography-tandem mass spectrometry. *Environmental Science: Processes & Impacts*, *20*(12), 1716–1727. https://doi.org/10.1039/C8EM00390D

Riml, J., & Wörman, A. (2011). Response functions for in-stream solute transport in river networks. *Water Resources Research*, *47*(6), W06502. https://doi.org/10.1029/2010WR009412

Riml, J., Wörman, A., Kunkel, U., & Radke, M. (2013). Evaluating the fate of six common pharmaceuticals using a reactive transport model: Insights from a stream tracer test. *Science of the Total Environment*, *458–460*, 344–354. https://doi.org/10.1016/j.scitotenv.2013.03.077

Romeijn, P., Hannah, D. M., & Krause, S. (2021). Macrophyte controls on urban stream microbial metabolic activity. *Environmental Science & Technology*, *55*(8), 4585–4596. https://doi.org/10.1021/acs.est.0c02854

Runkel, R. L. (1998). One-dimensional transport with inflow and storage (OTIS): A solute transport model for streams and rivers. (98-4018). Retrieved from http://pubs.er.usgs.gov/publication/wri984018

19447973, 2023, 7, Downloaded from https://agupubs.onlinelibrary.wiley.com/doi/10.1029/2022WR034203 by Paul Scherrer Institut PSI, Wiley Online Library on [20/07/2023]. See the Terms and Conditions (https://onlinelibrary.wiley.com/terms-and-conditions) on Wiley Online Library for rules of use; OA articles are governed by the applicable Creative Commons License

Runkel, R. L. (2002). A new metric for determining the importance of transient storage. *Journal of the North American Benthological Society*, *21*(4), 529–543. https://doi.org/10.2307/1468428

Ryan, R. J., Packman, A. I., & Welty, C. (2004). Estimation of solute transport and storage parameters in a stream with anthropogenically produced unsteady flow and industrial bromide input. *Water Resources Research*, *40*(1), W01602. https://doi.org/10.1029/2003wr002458

Salehin, M., Packman, A. I., & Wörman, A. (2003). Comparison of transient storage in vegetated and unvegetated reaches of a small agricultural stream in Sweden: Seasonal variation and anthropogenic manipulation. *Advances in Water Resources*, *26*(9), 951–964. https://doi.org/10.1016/S0309-1708(03)00084-8

Saltelli, A. (2002). Making best use of model evaluations to compute sensitivity indices. *Computer Physics Communications*, *145*(2), 280–297. https://doi.org/10.1016/S0010-4655(02)00280-1

Schaper, J. L., Posselt, M., Bouchez, C., Jaeger, A., Nuetzmann, G., Putschew, A., et al. (2019). Fate of trace organic compounds in the hyporheic zone: Influence of retardation, the benthic biolayer, and organic carbon. *Environmental Science & Technology*, *53*(8), 4224–4234. https://doi.org/10.1021/acs.est.8b06231

Schaper, J. L., Seher, W., Nutzmann, G., Putschew, A., Jekel, M., & Lewandowski, J. (2018). The fate of polar trace organic compounds in the hyporheic zone. *Water Research*, *140*, 158–166. https://doi.org/10.1016/j.watres.2018.04.040

Schmadel, N. M., Ward, A. S., Kurz, M. J., Fleckenstein, J. H., Zarnetske, J. P., Hannah, D. M., et al. (2016). Stream solute tracer timescales changing with discharge and reach length confound process interpretation. *Water Resources Research*, *52*(4), 3227–3245. https://doi.org/10.1002/2015WR018062

Schmid, B. H. (2003). Temporal moments routing in streams and rivers with transient storage. *Advances in Water Resources*, *26*(9), 1021–1027. https://doi.org/10.1016/S0309-1708(03)00086-1

Schmidt, C., Musolff, A., Trauth, N., Vieweg, M., & Fleckenstein, J. H. (2012). Transient analysis of fluctuations of electrical conductivity as tracer in the stream bed. *Hydrology and Earth System Sciences*, *16*(10), 3689–3697. https://doi.org/10.5194/hess-16-3689-2012

Schwientek, M., Guillet, G., Rügner, H., Kuch, B., & Grathwohl, P. (2016). A high-precision sampling scheme to assess persistence and transport characteristics of micropollutants in rivers. *Science of the Total Environment*, *540*, 444–454. https://doi.org/10.1016/j.scitotenv.2015.07.135

Shannon, C. E. (1948). A mathematical theory of communication. *The Bell System Technical Journal*, *27*(3), 379–423. https://doi.org/10.1002/j.1538-7305.1948.tb01338.x

Sheets, R. A., Darner, R. A., & Whitteberry, B. L. (2002). Lag times of bank filtration at a well field, Cincinnati, Ohio, USA. *Journal of Hydrology*, *266*(3), 162–174. https://doi.org/10.1016/S0022-1694(02)00164-6

Sobol, I. M. (2001). Global sensitivity indices for nonlinear mathematical models and their Monte Carlo estimates. *Mathematics and Computers in Simulation*, *55*(1), 271–280. https://doi.org/10.1016/S0378-4754(00)00270-6

Van Rossum, G., & Drake, F. L. (2003). *Python language reference manual*. Network Theory Limited.

Vogt, T., Hoehn, E., Schneider, P., Freund, A., Schirmer, M., & Cirpka, O. A. (2010). Fluctuations of electrical conductivity as a natural tracer for bank filtration in a losing stream. *Advances in Water Resources*, *33*(11), 1296–1308. https://doi.org/10.1016/j.advwatres.2010.02.007

Wagner, B. J., & Harvey, J. W. (1997). Experimental design for estimating parameters of rate-limited mass transfer: Analysis of stream tracer studies. *Water Resources Research*, *33*(7), 1731–1741. https://doi.org/10.1029/97WR01067

Ward, A. S., Kelleher, C. A., Mason, S. J. K., Wagener, T., McIntyre, N., McGlynn, B., et al. (2017). A software tool to assess uncertainty in transient-storage model parameters using Monte Carlo simulations. *Freshwater Science*, *36*(1), 195–217. https://doi.org/10.1086/690444

Ward, A. S., Wondzell, S. M., Schmadel, N. M., Herzog, S., Zarnetske, J. P., Baranov, V., et al. (2019). Spatial and temporal variation in river corridor exchange across a 5th-order mountain stream network. *Hydrology and Earth System Sciences*, *23*(12), 5199–5225. https://doi.org/10.5194/hess-23-5199-2019

Wörman, A. (2000). Comparison of models for transient storage of solutes in small streams. *Water Resources Research*, *36*(2), 455–468. https://doi.org/10.1029/1999WR900281

Wörman, A., Packman, A. I., Johansson, H., & Jonsson, K. (2002). Effect of flow-induced exchange in hyporheic zones on longitudinal transport of solutes in streams and rivers. *Water Resources Research*, *38*(1), 2-1–2-15. https://doi.org/10.1029/2001WR000769

Wörman, A., & Wachniew, P. (2007). Reach scale and evaluation methods as limitations for transient storage properties in streams and rivers. *Water Resources Research*, *43*(10), W10405. https://doi.org/10.1029/2006WR005808

Wu, L., Gomez-Velez, J. D., Krause, S., Singh, T., Wörman, A., & Lewandowski, J. (2020). Impact of flow alteration and temperature variability on hyporheic exchange. *Water Resources Research*, *56*(3), e2019WR026225. https://doi.org/10.1029/2019WR026225

19447973, 2023, 7, Downloaded from https://agupubs.onlinelibrary.wiley.com/doi/10.1029/2022WR034203 by Paul Scherrer Institut PSI, Wiley Online Library on [20/07/2023]. See the Terms and Conditions (https://onlinelibrary.wiley.com/terms-and-conditions) on Wiley Online Library for rules of use; OA articles are governed by the applicable Creative Commons License